Core-coupled protons, f_{7/2} intruder states, and competing g_{9/2} proton and neutron structures in ^{65,67}Cu

C. J. Chiara, I. Stefanescu, W. B. Walters, S. Zhu, R. V. F. Janssens, M. P. Carpenter, R. Broda, B. Fornal, A. A. Hecht, N. Hoteling, E. G. Jackson, B. P. Kay, W. Królas, T. Lauritsen, E. A. McCutchan, T. Pawłat, D. Seweryniak, X. Wang, A. Wöhr, and J. Wrzesiński

Phys. Rev. C **85**, 024309 — Published 13 February 2012

DOI: 10.1103/PhysRevC.85.024309

Core-coupled protons, $f_{7/2}$ intruder states, and competing $g_{9/2}$ proton and neutron structures in ^{65,67}Cu

C. J. Chiara,[1,2] I. Stefanescu,[1,2] W. B. Walters,[1] S. Zhu,[2] R. V. F. Janssens,[2]
M. P. Carpenter,[2] R. Broda,[3] B. Fornal,[3] A. A. Hecht,[1,2,*] N. Hoteling,[1,2]
E. G. Jackson,[2,†] B. P. Kay,[2,‡] W. Królas,[3] T. Lauritsen,[2] E. A. McCutchan,[2,§]
T. Pawłat,[3] D. Seweryniak,[2] X. Wang,[2,4,¶] A. Wöhr,[1,2,4] and J. Wrzesiński[3]

[1]*Department of Chemistry and Biochemistry, University of Maryland, College Park, Maryland 20742, USA*

[2]*Physics Division, Argonne National Laboratory, Argonne, Illinois 60439, USA*

[3]*Niewodniczański Institute of Nuclear Physics PAN, PL-31-342 Kraków, Poland*

[4]*Department of Physics, University of Notre Dame, Notre Dame, Indiana 46556, USA*

Abstract

The nuclei ^{65,67}Cu were studied in reactions between a 430-MeV ^{64}Ni beam and a thick ^{238}U target with the Gammasphere array. Decay schemes for both nuclei have been extended, with spin and parity assignments of observed states constrained by measured gamma-ray angular distributions and correlations. Positive-parity level structures, based on $p_{3/2}$ protons coupled to negative-parity states in the Ni cores, have been identified above the known $9/2^+$ states. In ^{67}Cu, a negative-parity dipole band built upon a $\pi f_{7/2}^{-1}$ state has been observed, as were two shorter negative-parity sequences. A qualitative description of the level structures has been obtained through comparison with systematics of the odd-A $^{57-71}$Cu isotopes and with states in the neighboring even-even Ni and Zn cores. Shell-model calculations using JUN45 and jj44b effective interactions were performed for ^{65,67}Cu, with jj44b providing overall better agreement with the data. Both are limited, however, by the restriction that the $f_{7/2}$ and $g_{9/2}$ orbitals are not available simultaneously in the basis. Proton $f_{7/2}$ and neutron $g_{9/2}$ orbitals are required for the full negative-parity spectrum of states, while $g_{9/2}$ protons and neutrons are both important for positive-parity levels. The latter states are found to be better described in terms of weak coupling of a proton to the Ni core.

PACS numbers: 23.20.Lv, 23.20.En, 21.60.Cs, 27.50.+e

*Present address: Department of Chemical and Nuclear Engineering, University of New Mexico, Albu-

querque, New Mexico 87131-0001, USA
[†]Present address: Department of Physics, University of Massachusetts, Lowell, Massachusetts 01854, USA
[‡]Present address: Department of Physics, University of York, Heslington, York YO10 5DD, UK
[§]Present address: National Nuclear Data Center, Brookhaven National Laboratory, Upton, New York 11973-5000, USA
[¶]Present address: Department of Physics, Florida State University, Tallahassee, Florida 32306-4350, USA

I. INTRODUCTION

Nuclei in the neutron-rich Ni region present a challenge to modern shell-model calculations. The Cu isotopes have a single proton outside the $Z = 28$ Ni core, placing them within the proton $f_{5/2}p$ subshell. Taking a simplistic view of the occupation of orbitals with increasing neutron number leads to the expectation that the neutrons are predominantly confined to the $p_{3/2}$ orbital for $N = 28$ to 32, to the $f_{5/2}$ for $N = 33$ to 38, followed by the $p_{1/2}$ orbital, and finally, as N exceeds 40, to the $g_{9/2}$ subshell. Recent results from neutron-transfer studies on even-A stable Ni isotopes, however, indicate that the $p_{3/2}$, $f_{5/2}$, and $p_{1/2}$ orbitals are essentially filled in parallel [1]. Furthermore, the inversion of the $f_{5/2}$ and $p_{3/2}$ proton orbitals has been established for the ground state of ^{75}Cu [2]. Measurements of ground-state moments of the Cu isotopes have also revealed a more complex picture: Magnetic dipole moments for $N \leq 40$ were found to have values well below the expected Schmidt limits for a $\pi p_{3/2}$ ground state [3]. Comparisons of measured magnetic dipole and electric quadrupole moments with the results of shell-model calculations using the GXPF1 [4], GXPF1A [5], and JUN45 [6] interactions indicate that excitations of nucleons from the $f_{7/2}$ subshell across the $Z, N = 28$ shell gaps are necessary to reproduce the measured values for the Cu isotopes with $A = 63$ or less, while the $g_{9/2}$ neutron is important in describing the ground state of ^{69}Cu [7]. The latter observation disagrees with earlier findings that the $g_{9/2}$ neutron is *not* needed to adequately describe the ^{69}Cu ground-state magnetic moment [8–10]. The complexity of these findings invite additional scrutiny of the Cu nuclei.

With the possible influence of both $f_{7/2}$ and $g_{9/2}$ orbitals on the structure of these nuclei, full shell-model calculations without truncations consequently require larger valence spaces and can become intractably difficult. The evolution of codes designed to take advantage of advances in computing speed and power will ultimately allow consideration of these large dimensions. To this end, detailed level structures of ^{65,67}Cu, especially in comparison with the reasonably well established decay schemes of their corresponding cores, ^{64,66}Ni, represent a valuable addition to the available data for testing new effective interactions.

II. PREVIOUS STUDIES OF ^{65,67}CU

Despite the proximity of ^{65,67}Cu to the line of stability—^{65}Cu is, in fact, a stable nucleus—high-spin states have not been studied very extensively in either nucleus. In ^{65}Cu, the highest-spin states for which gamma-ray spectroscopy was performed are states at 2999 and 3278 keV with tentative $11/2^-$ assignments and a $9/2^+$ level at 2535 keV using $(n, n'\gamma)$ reactions, with no gamma rays observed feeding them from higher-lying structures [11, 12]. Lower-spin levels up to 8.5 and 15.5 MeV were identified, respectively, through gamma deexcitations in (γ, γ') [13, 14] and $(n, n'\gamma)$ [11] reactions, and without gamma-ray detection in (p, p') [15] and $(\vec{d},^3\mathrm{He})$ [16] reactions (see also Ref. [17]).

The most extensive high-spin gamma-ray spectroscopy for ^{67}Cu was the study by Asai *et al.* [18], in which ^{67}Cu was produced in deep-inelastic collisions of a ^{76}Ge beam with a ^{198}Pt target. Beamlike reaction products exited the target and were implanted in a downstream Si detector, with subsequent gamma decays detected by Ge detectors that surrounded the Si but were shielded from direct view of the target. This "isomer-scope" was sensitive to decays occurring about 1 ns or more after the collision. In their work, a level scheme comprised of eight gamma rays and five excited states up to 3464 keV was constructed. The latter state was determined to be isomeric with an estimated half-life of $0.6 < t_{1/2} < 2.4$ ns, and all observed gamma rays followed its decay.

III. EXPERIMENTAL DETAILS

Excited states up to moderate spins in ^{65,67}Cu were populated in (deep-)inelastic reactions between a ^{64}Ni beam and a ^{238}U target. The 430-MeV beam was provided by the ATLAS facility at Argonne National Laboratory in ∼0.3-ns pulses separated by 412 ns. The enriched ^{238}U target of 55-mg/cm^2 thickness, tilted at an angle of 27° from the vertical, provided sufficient material to stop all reaction products. Emitted gamma rays were detected with the Gammasphere array of Compton-suppressed HPGe detectors [19], with 100 in place for this experiment. A total of 2.5×10^9 events satisfying the trigger condition of a "clean" (Compton-suppressed) gamma-ray fold of three or greater were recorded.

IV. ANALYSIS

The procedure for sorting events into prompt (P) and delayed (D) coincidence histograms is described in previous publications based on this experiment [20–24]. Events were unfolded into triple gamma-ray coincidences. Three-dimensional *cubes* of the gamma-ray energies E_γ were incremented if the three transitions satisfied certain relative time conditions. For the ^{65,67}Cu analysis, this primarily required all three decays to be prompt; i.e., that they were all detected within a 40-ns window centered around the beam burst (PPP cube). The coincidence events involving delayed transitions (PPD, PDD, and DDD cubes [24]) were also investigated for the possible presence of longer-lived (i.e., $\gtrsim$20 ns) decays in both nuclei, but none were identified. The RADWARE analysis code LEVIT8R [25] was used to project double-gated, background-subtracted spectra from the coincidence cube.

An angular-correlation (AC) analysis was performed to determine the multipolarities of transitions in ^{65,67}Cu. For this purpose, pairs of Ge detectors were divided, according to the angle ψ between them, into ten groups with average values 20.3°, 34.9°, 40.6°, 53.8°, 60.2°, 67.0°, 70.6°, 73.6°, 80.1°, and 86.5°. Angles $\psi > 90°$ were binned as $180° - \psi$. A set of two-dimensional coincidence *matrices* was created where each matrix corresponded to one of the ten angle groups. For every pair of prompt gamma rays with energies $E_{\gamma 1}$, $E_{\gamma 2}$ and relative angle ψ, the AC matrix for the angle group including ψ was incremented symmetrically at cells $(E_{\gamma 1}, E_{\gamma 2})$ and $(E_{\gamma 2}, E_{\gamma 1})$. Background-subtracted, angle-dependent spectra were projected from each of the ten AC matrices by gating on transitions with known multipolarities in ^{65,67}Cu. Peak areas for coincident gamma rays were measured and corrected for efficiency. This correction incorporates both the efficiency for the Ge detector itself under these experimental conditions, and a normalization for the number of pairs of detectors in the specific angle group. The resulting intensity $W(\psi)$ was least-squares fitted with the standard Legendre-polynomial expression $W(\psi) = a_0[1 + a_2 P_2(\cos\psi) + a_4 P_4(\cos\psi)]$ to determine the AC coefficients a_2 and a_4, which are then used to infer the multipolarity of the second transition. Table I lists some representative, expected values for various combinations of multipolarities.

In the case of ^{65}Cu, many of the AC results were found to be inconclusive, due primarily to the difficulty in finding strong, uncontaminated gating transitions with established multipolarities. Several participants in the present study were also involved in a separate experiment

TABLE I: Angular correlation (AC) coefficients a_2, a_4 expected for different combinations of transitions with specific unique multipolarities. The AC for a given gamma-ray pair is identical regardless of which is the gating transition. $M1$ transitions have coefficients identical to their $E1$ counterparts, but an $E2$ admixture with the former alters these values. The calculated coefficients given here are representative values for the initial and final spins listed. Intervening transitions can affect the AC coefficients, and there is a spin dependence when non-stretched transitions are involved.

transitions	$9/2 \rightarrow 3/2$ $E3$	$9/2 \rightarrow 5/2$ $E2$	$9/2 \rightarrow 7/2$ $E1$
$13/2 \rightarrow 9/2$ $E2$	$0.179, -0.004$	$0.102, 0.009$	$-0.071, 0$
$11/2 \rightarrow 9/2$ $E1$	$-0.125, 0$	$-0.071, 0$	$0.050, 0$
$9/2 \rightarrow 9/2$ $E1$	$0.333, 0$	$0.190, 0$	$-0.133, 0$

with Gammasphere involving a high-energy ^{48}Ca beam on a thin ^{26}Mg target, which produced ^{65}Cu as one of the reaction channels. (Details of this experiment will be provided separately [26].) Here, the angular momenta of the reaction products had a well-defined orientation with respect to the beam direction, enabling a double-gated angular-distribution (AD) measurement. Spectra were generated from events in which two coincident gamma rays, detected at any angles, satisfied a particular set of energy gates; one-dimensional histograms were incremented at the energy of a third gamma ray in the event, if it was recorded in designated rings of Gammasphere detectors. The rings were separated into seven groups with average angles $\theta = 17^\circ$, 35°, 50°, 58°, 70°, 80°, and 90° with respect to the beam axis. The symmetry of Gammasphere around 90° was exploited and rings at angles θ and $180^\circ - \theta$ were combined. Background subtraction and generation of error spectra were performed according to the prescription given in Ref. [27]. Peaks for transitions of interest were fitted at the seven angles, corrected for efficiency, and compared to calculated angular distributions having the same form as the expression for angular correlations. An alignment parameter $\sigma/I = 0.5$ was assumed in the calculations, as this yielded good agreement for known $E2$ and $E1$ transitions. Some representative AD coefficients are given in Table II.

TABLE II: Angular distribution coefficients a_2 and a_4 expected for transitions with specific unique multipolarities. $M1$ transitions have coefficients identical to their $E1$ counterparts, but an $E2$ admixture with the former alters these values. The calculated coefficients given here are representative values for the initial and final spins listed. A spin-alignment parameter $\sigma/I = 0.5$ is assumed.

transition	a_2	a_4
$13/2 \rightarrow 9/2$ $E2$	0.207	-0.027
$9/2 \rightarrow 7/2$ $E1$	-0.165	0
$7/2 \rightarrow 7/2$ $E1$	0.247	0

V. RESULTS

A. ^{65}Cu level scheme

A level scheme for ^{65}Cu, up to moderate spins, was constructed based on analysis of the PPP cube. It builds upon the levels found in the literature (Ref. [17], and references therein). Representative double-gated, background-subtracted coincidence spectra confirming part of the previously existing decay scheme are given in Fig. 1. Several new lines are identified in the spectra double gated on 1115/979 keV [Fig. 1(a)] and on 1482/1052 keV [Fig. 1(b)]. Subsequently double gating on pairs of these lines, such as the 1126- and 415-keV transitions [Fig. 1(c)], reveals that these comprise a band structure built upon the previously established 2534-keV state. The level scheme for ^{65}Cu, deduced from these coincidence relationships as well as from transition intensity balances and consistency of gamma-ray energy sums, is presented in Fig. 2. The observed gamma rays in the portion of the level scheme above the 2534-keV $9/2^+$ state (red in online version) are new to this work. Properties of these levels and gamma rays are summarized in Table III. Of the previously identified levels below 2 MeV [17], two are not observed in this work: the 771-keV $1/2^-$ and 1725-keV $3/2^-$ levels. This is likely because of their low spins.

Spins and parities (I^π) have been assigned for most states identified in ^{65}Cu—see Fig. 2. Those considered tentative are indicated in parentheses. These assignments are based on the evaluated data of Ref. [17] (primarily for the lower-lying states) and on AD measurements performed in this work, as detailed below. Figure 3 provides several examples of the AD

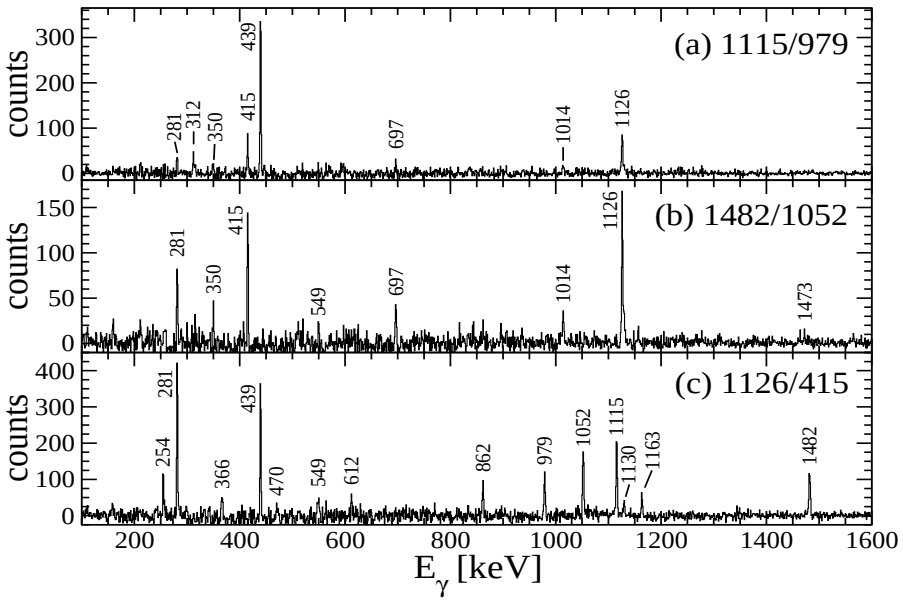

FIG. 1: Background-subtracted coincidence spectra double gated in the PPP cube on transitions at (a) 1115/979 keV, (b) 1482/1052 keV, and (c) 1126/415 keV. Peaks identified in ^{65}Cu are labelled with their energies in keV. Spectra are at 1 keV/channel.

data compared to theoretical curves for the assigned multipolarities.

The I^π assignments for the ground, 1116-keV, 1482-keV, and 1624-keV states have been well established as $3/2^-$, $5/2^-$, $7/2^-$, and $5/2^-$, respectively, through several experimental techniques (see summary in Ref. [17]). Our AD data confirm the $M1/E2$ multipolarities of the 366- and 1115-keV transitions connecting the 1482-keV, 1116-keV, and ground states [see Table III and Fig. 3(h)]. A large mixing ratio, $\delta = -0.450(16)$, was adopted for the 1115-keV gamma ray in Ref. [17]. From the best fit with the assumption $\sigma/I = 0.5$, a lower value of $\delta \approx -0.1$ is deduced. However, this difference is easily taken into account if spin alignment is less than expected and some deorientation occurs before the corresponding state decays. Specifically, with $\sigma/I \approx 0.7$, the best fit to the data would yield the same mixing ratio as found in the literature.

The evaluation of Ref. [17] lists three unique levels between 2525 and 2535 keV. Two of these, at 2525.74(21) and 2533.9(4) keV, were associated with $L = 4$ transfer from 0^+ target ground states [(α, p) [28], (t, α) [29], (^{3}He,d) [30], and (α, t) [31] reactions], $L = 3$ from $3/2^-$ ground states [(p, p') [32], (α, α') [33], (t, p) [34], and (d, d') [35] reactions], or both. In addition, for the former of these two levels, a 1044-keV gamma ray observed in $(p, p'\gamma)$ was

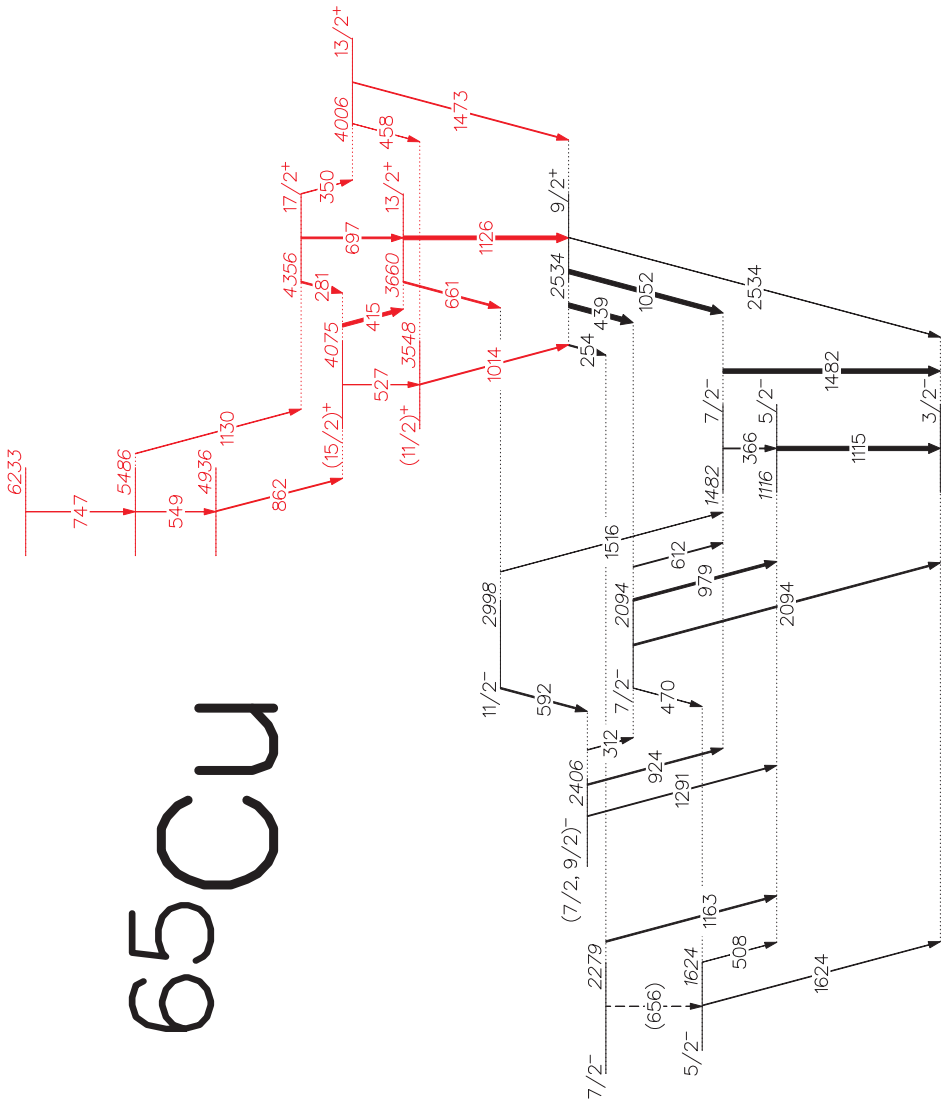

FIG. 2: (Color online) Level scheme of ^{65}Cu deduced from the PPP cube in this work. Gamma rays above the 2534-keV $9/2^+$ state are newly observed. Energies of states (in italics) and transitions are labelled in keV. Tentative spins, parities, and gamma-ray energies are given in parentheses. Gamma-ray intensities are represented by the widths of the arrows.

placed in Ref. [36] feeding the 1482-keV $7/2^-$ state, while the latter was identified in (p,γ) [37] and $(n,n'\gamma)$ [11] by gamma decay to $7/2^-$ levels at 1482, 2095, and 2279 keV. Both of these levels are consistent with an $I^\pi = 9/2^+$ assignment. The third state, at 2533.04(15) keV, was observed in (p,γ) [37] and $(n,n'\gamma)$ [11] reactions to decay to $1/2^-$ and $3/2^-$ levels. The decay to low-spin states only, and the presence of two resolved gamma lines in those data, make it clear that the 2533.04-keV level is distinct from the other two. Most of the

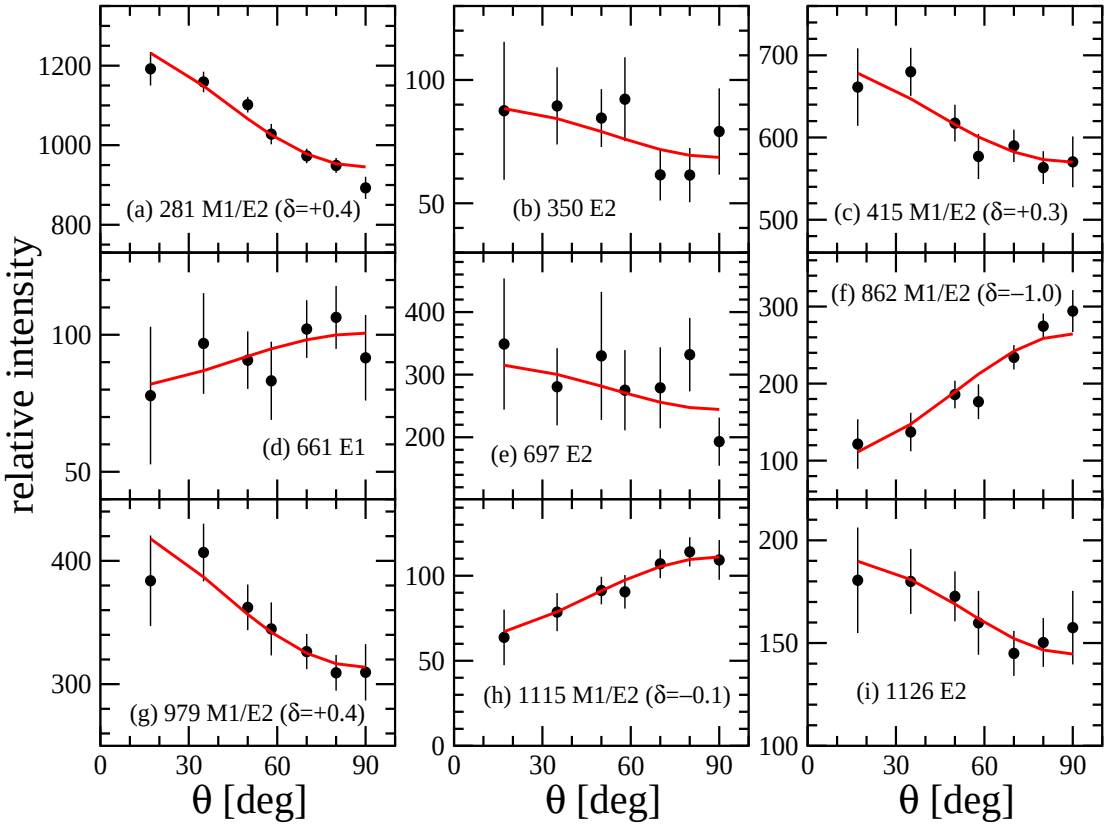

FIG. 3: (Color online) Measured angular distributions (filled circles) in ^{65}Cu for the transitions labelled in each panel. The best-fit calculated curves for the multipolarities given in the figure are shown as solid lines.

transfer reactions did not have sufficient energy resolution to reliably infer the presence of two $9/2^+$ states within ∼8 keV of each other (the exception being Ref. [28] which identified only a single state with a 2-keV uncertainty); this conclusion was instead based on the high-resolution gamma-ray energy measurements. In the present work, the existence of this $9/2^+$ doublet was investigated. The 254-, 439-, and 1052-keV gamma rays observed in $(n, n'\gamma)$ and (p, γ) were, likewise, seen here (Fig. 2). The proposed 1044-keV decay to the 1482-keV level also should have been visible, but was not, casting doubt on the existence of a $9/2^+$ doublet at ∼2530 keV. It should be noted that the 808- and 1762-keV gamma rays found to depopulate the 2533.04-keV level in Ref. [37] were not observed here either, but this is consistent with that level having a low spin and not being strongly populated in inelastic reactions. Therefore, only a single level at 2534 keV is present in the decay scheme of Fig. 2, with $I^\pi = 9/2^+$ quantum numbers.

The 439- and 254-keV gamma rays depopulating the 2534-keV state were both found to be consistent with a stretched-dipole character (see Table III). The two states they feed at 2094 and 2279 keV, respectively, had both been previously assigned $I^\pi = (7/2)^-$ [17] based on a comparison with Hauser-Feshbach theory in (p,γ) [37] and $L = 3$ transfer in $(d,^3\mathrm{He})$ [38] and (t,α) [29] reactions. The previous determination of negative parity for these states implies that the gamma rays must be parity-changing $E1$ transitions, and the spins of both final levels are confirmed to be 7/2. The quality of the AD fit for the 1052-keV transition is poorer than those for the 439- and 254-keV gamma rays, but is nevertheless found to be consistent with the expected $E1$ deexcitation between the 2534-keV $9/2^+$ and 1482-keV $7/2^-$ levels.

As can be seen from Fig. 3, the ADs for the 1126-, 697-, and 350-keV transitions are all consistent with an $E2$ multipolarity. These lead to I^π assignments of $13/2^+$ for the 3660- and 4006-keV levels, and $17/2^+$ for the state at 4356 keV. Although the AD curves for the 281- and 415-keV gamma rays are peaked at 0° like an $E2$ transition, they are in agreement with $\Delta I = 1$ $M1/E2$ assignments with mixing ratios $\delta \approx +0.4$ and $+0.3$, respectively, with a 697-keV crossover transition of $E2$ character. The possibility that one of those two gamma rays has $\Delta I = 0$ $M1/E2$ character and the other stretched $E2$ multipolarity cannot be ruled out, however, so the 15/2 spin of the intermediate state at 4075 keV should be viewed as tentative. Regardless, positive parity is established for this level. The 3548-keV state is fed by ones assigned $I^\pi = 13/2^+$ and $(15/2)^+$, and decays to the $9/2^+$ 2534-keV level. The most likely assignment is, therefore, a spin of 11/2 or 13/2, with positive parity; the former spin is preferred, because the latter assignment would make the 3548-keV level the yrast $13/2^+$ state, despite it carrying several times less intensity than the 3660-keV $13/2^+$ state.

The 549- and 747-keV gamma rays appear to form the beginnings of a band structure that decays into the positive-parity states. No AD information could be obtained for either of those gamma rays or for the 1130-keV linking transition, but the best AD fit for the 862-keV decay is for a $\Delta I = 1$ $M1/E2$ assignment with a mixing ratio of $\delta \approx -1.0$ [Fig. 3(f)], suggesting that this structure may also have positive parity.

A level at 3003(5) keV was identified in the (α,p) transfer study by Nybø *et al.* [28] and assigned $I^\pi = (11/2^-)$ based on a DWBA analysis. In the present study, a 661-keV gamma ray was observed between the 3660-keV, $13/2^+$ state and one at 2998 keV; the latter may correspond to the one seen in Ref. [28]. The AD for this gamma ray is consistent with a

$\Delta I = 1$ dipole character [Fig. 3(d)], indicating that the 2998-keV level has spin 11/2. This level decays by a 1516-keV transition to the 1482-keV, $7/2^-$ state, making negative parity more likely. The 2998-keV level has, thus, been assigned $I^\pi = 11/2^-$, in agreement with the (α, p) work [28]. The state at 2406 keV, fed by the $11/2^-$ and decaying to $7/2^-$ and $5/2^-$ levels, is most likely of negative parity as well with spin 7/2 or 9/2.

B. ^{67}Cu level scheme

The ^{67}Cu level scheme proposed in Ref. [18] was used as a starting point for the present analysis. A double coincidence gate on the known 1115- and 554-keV transitions produced the spectrum in Fig. 4(a). The 833-, 861- and 100-keV gamma rays from Ref. [18] are observed, and several new transitions have been identified. The spectrum double gated on two of these, the 524– and 775-keV transitions, is shown in Fig. 4(b). With these spectra, all gamma rays observed in Ref. [18] were confirmed. Additionally, the level scheme has been extended above the known 3463-keV, ∼1-ns isomer. Figure 5 provides the ^{67}Cu level scheme deduced in this work from the coincidence relationships, intensity balances, and energy sums for the observed gamma rays; the newly established portion of the level scheme is indicated in red (online version). Properties of these levels and gamma rays are also summarized in Table IV. Of the previously identified levels below 2 MeV [28], three are not seen in this work: the 1169-keV $(1/2)^-$, 1633-keV $(5/2)^-$, and 1937-keV $3/2^-$ levels. It is somewhat surprising that no gamma-ray cascades passing through the 1633-keV state were observed, considering that there are several identified levels that could directly populate one with $I^\pi = 5/2^-$ (see Fig. 5).

Two gamma rays with energies 793 and 614 keV were identified as populating the 2503-keV level. The former is also in coincidence with gamma rays above the 3363-keV state, but not with the 861-keV transition. This suggests that there is an unobserved 67-keV gamma ray in cascade with the one at 793 keV carrying intensity parallel to the 861-keV branch. The Gammasphere array has low efficiency at energies below 100 keV, and the observed coincidence spectra are consistent with the expected intensity for the 67-keV transition based on the proposed 67-793-keV decay path. Note that the order of the 67- and 793-keV transitions could be interchanged, so the level at 3296 keV should be considered tentative. However, in Fig. 12 of the (α, p) study by Nybø *et al.* [28] there is an unlabelled peak

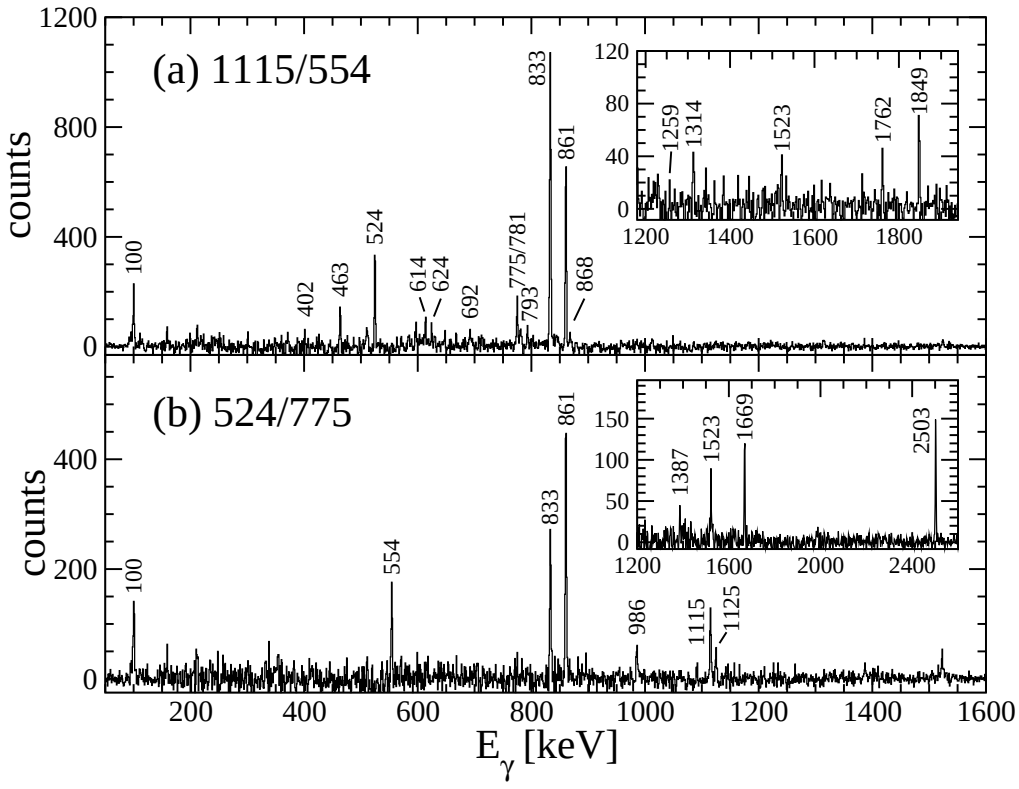

FIG. 4: Background-subtracted coincidence spectra double gated in the PPP cube on transitions at (a) 1115/554 keV and (b) 524/775 keV. Peaks identified in ^{67}Cu are labelled with their energies in keV. Spectra (a) and (b) are at 1 keV/channel; the insets, which display the high-energy regions of the same spectra, are provided with a dispersion of 2 keV/channel.

between those marked as 13 (3277 keV) and 14 (3334 keV) that would correspond to a level at about 3298 keV. From Ref. [28], it is not clear why this peak was not associated with a level in ^{67}Cu but, if real, this would support the placement proposed here of the 793-keV transition depopulating a state at 3296 keV.

Several peaks are observed at higher energies in the 1115/554-keV coincidence spectrum [inset of Fig. 4(a)]. Double gating on these higher-energy lines and the 1115-, 554-, and 1669-keV transitions reveals new structures in ^{67}Cu. Figure 6(a), for example, presents the spectrum in coincidence with the 1115- and 1259-keV gamma rays [the latter is in rather weak coincidence with the 554-keV gamma ray, hence the small peak in the inset of Fig. 4(a)]; a prominent 1246-keV peak is observed, as well as several at lower energies. Summing gates on 1115/1246- and 571/1246-keV lines yields the spectrum in Fig. 6(b), in which a

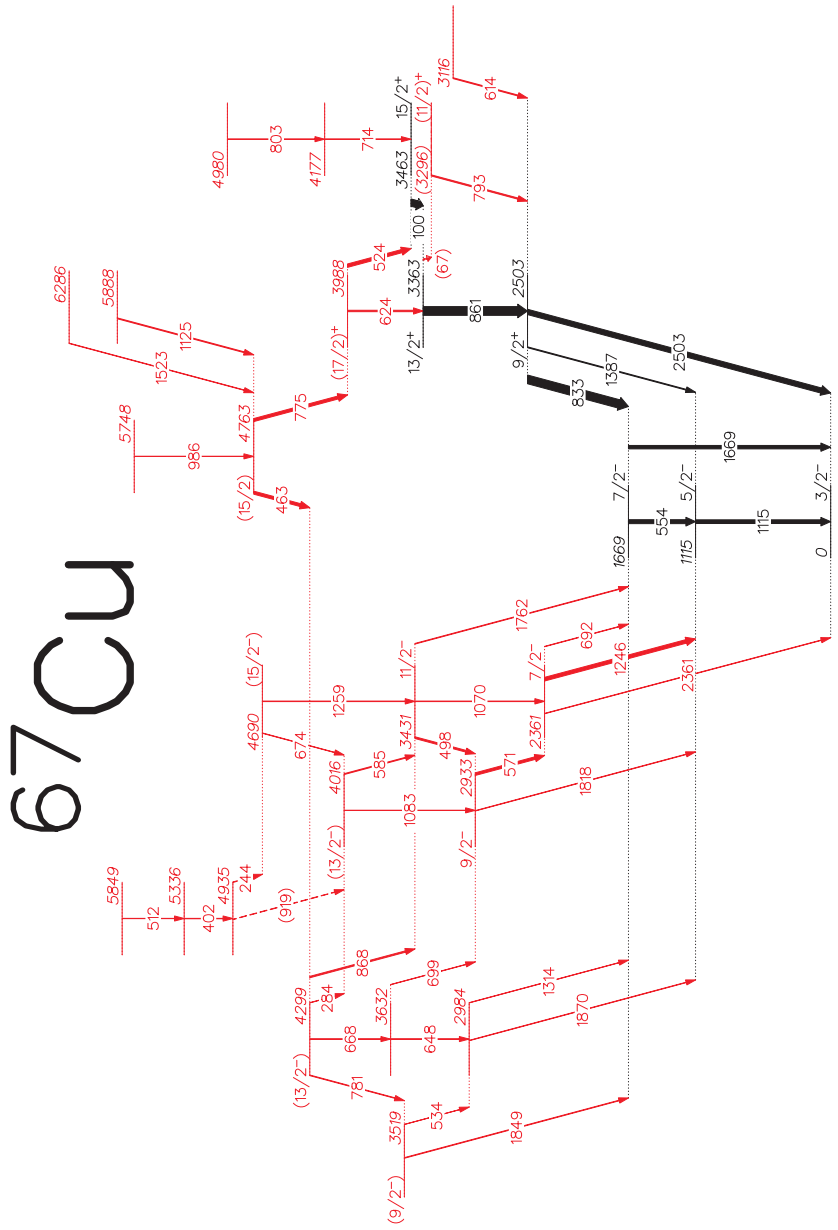

FIG. 5: (Color online) Level scheme of ^{67}Cu deduced from the PPP cube in this work. Gamma rays other than those following the decay of the 3463-keV $15/2^+$ state are newly observed (red online). Energies of states (in italics) and transitions are labelled in keV. Tentative spins, parities, and gamma-ray energies are given in parentheses. Gamma-ray intensities are represented by the widths of the arrows.

number of previously unknown gamma rays are identified. These are organized into several band structures as proposed in the enclosed region in Fig. 5.

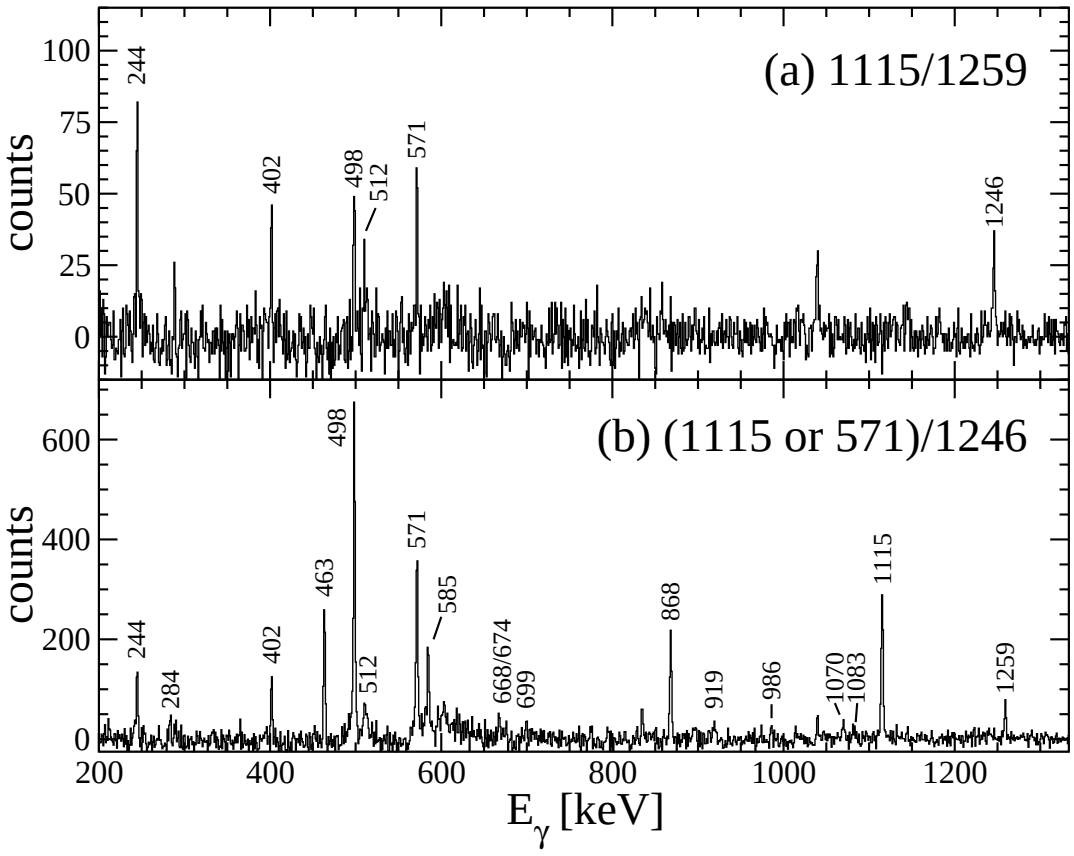

FIG. 6: Background-subtracted coincidence spectra double gated in the PPP cube on transitions at (a) 1115/1259 keV and (b) (1115 or 571)/1246 keV. Peaks identified in ^{67}Cu are labelled with their energies in keV. Spectra are at 1 keV/channel.

Asai *et al.* assigned firm spins and parities to all of the ^{67}Cu levels identified in Ref. [18], based on gamma-ray angular distributions in their work and on results from (α, p) [28], $(d,^3\mathrm{He})$ [38], and (t, p) [34] transfer studies. The results of the AC fits from the current work are presented in Table IV, with a representative sample of the data and theoretical curves for the assigned multipolarities shown in Fig. 7. Typically only $E2$, $M1$, and $E1$ multipolarities were considered, although there are exceptions such as the known 2503-keV $E3$ and 1387-keV $M2$ transitions depopulating the 2503-keV state. Our AC measurements were found to be consistent with the assignments proposed in Ref. [18]. From a best fit to the 861-keV $E2$ − 1115-keV $M1/E2$ AC [see Fig. 7(b) and Table IV], the mixing ratio for

the latter transition was determined to be $\delta = -0.19$. This value was used when calculating theoretical curves for comparison with the correlations between the 1115-keV gamma ray and

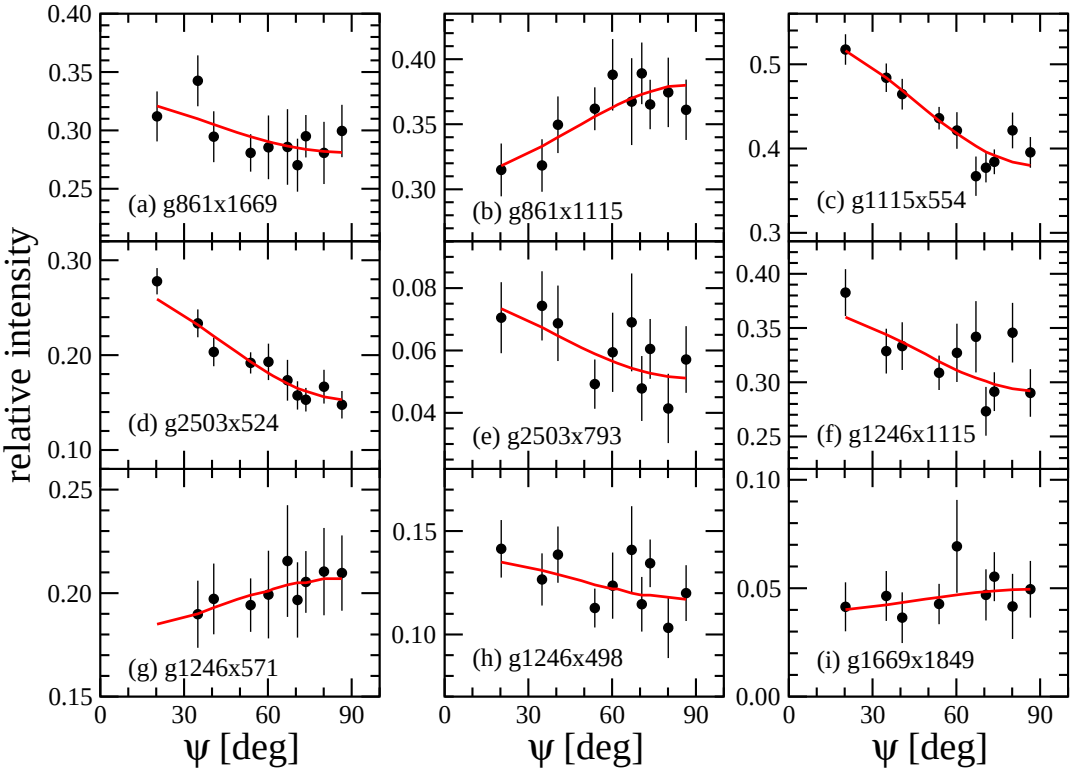

FIG. 7: (Color online) Measured angular correlations (filled circles) in ^{67}Cu for the transition pairs labelled in each panel, where 'g' and 'x' signify the energies of the gated and examined gamma rays, respectively. The best-fit calculated curves are given as solid lines. The data points at 20.3° in (g) and at 67.0° in (i) were eliminated because of unreliable peak fits.

The 2503-keV $E3$ − 524-keV AC [Fig. 7(d)] is peaked at 0°, ruling out $\Delta I = 1$ $E1$ character for the 524-keV transition, but the slope is also too steep for it to be an $E2$ transition and is somewhat steeper than expected for a $\Delta I = 0$ $E1$ transition. The best agreement is for a $\Delta I = 0$ or 1 transition with mixed $M1/E2$ character. The 624-keV gamma ray is found to be consistent with $E2$ multipolarity, although a mixed $\Delta I = 1$ $M1/E2$ transition is also possible. The state at 3988 keV is, therefore, assigned positive parity and a tentative spin (17/2). The AC for the 2503-keV $E3$ − 793-keV pair [Fig. 7(e)] rules out a $\Delta I = 1$ $E1$ assignment for the 793-keV transition feeding the level at 2503 keV. A $\Delta I = 0$ $E1$ assignment is also unlikely as this would make the inferred 67-keV gamma

ray an $M2$ transition between $13/2^+$ and $9/2^-$ states. Although the 67-keV line was not observed in our data, the long lifetime this scenario implies would have been evident in the 861-keV decay from the same level. Thus, the 3296-keV state is assigned positive parity. It is tentatively given an (11/2) value as the most likely spin. With the addition of these two states, a positive-parity structure built upon the 2503-keV $9/2^+$ state that includes all spins from 9/2 to (17/2) has been identified for the first time in ^{67}Cu.

Two gamma rays with energies 803 and 714 keV were found to decay in sequence to the 3463-keV $15/2^+$ state. The AC fits for these transitions were inconclusive (Table IV), so no I^π assignments are proposed for the 4177- or 4980-keV states.

The 2361-keV level decays by a strong 1246-keV transition to the 1115-keV $5/2^-$ state and by weaker decays to the 1669-keV $7/2^-$ and $3/2^-$ ground states. The 1246-keV − 1115-keV AC [see Fig. 7(f) and Table IV], with the assumption that the latter is an $M1/E2$ transition with $\delta = -0.19$, yields best agreement with calculated AC's when the 1246-keV gamma ray is either of $\Delta I = 1$ $M1/E2$ ($\delta = +0.07$) or $\Delta I = 0$ $M1/E2$ ($\delta = -0.67$) character. In early (d,^{3}He) work by Zeidman and Nolen [38], a level at 2340(20) keV was observed with $L = 3$ transfer and a large spectroscopic factor, $C^2S = 3.1$, associated with the proton $f_{7/2}$ orbital. The level was consequently assigned as $I^\pi = 7/2^-$. The level observed here at 2361 keV is likely the same as the one observed in Ref. [38], and the AC result is consistent with the spin-parity assignments proposed in the latter work. Therefore, the $7/2^-$ assignment is adopted here as well.

With the multipolarity of the 1246-keV transition being established, it can be used as a gate to examine the members of the band built upon the 2361-keV $7/2^-$ state. Specifically, AC fits were possible for the 571- and 498-keV gamma rays. In the calculated AC, the 1246-keV gate is taken to be a $\Delta I = 1$ $M1/E2$ transition with $\delta = -0.07$. (The sign of the mixing ratio is reversed here compared to that determined above because the transition lies below the intermediate state separating the correlated gamma-ray pair rather than above it, as was true for the 1246-keV − 1115-keV AC.) The resulting fits for the 571- and 498-keV gamma rays indicate both are consistent with mixed $M1/E2$ multipolarity [see Figs. 7(g,h) and Table IV], giving the 2933- and 3431-keV states $I^\pi = 9/2^-$ and $11/2^-$ assignments, respectively. No other AC fits were possible within this band but, based on its organization as a strongly coupled band, the 4016- and 4690-keV states are tentatively assigned as the $(13/2^-)$ and $(15/2^-)$ continuation of the sequence.

Not much information can be obtained for the weak gamma rays within the structure on the far left of Fig. 5, but AC's were measurable for the 781- and 1849-keV gamma rays decaying in sequence from the state at 4299 keV [Table IV and Fig. 7(i)]. The 781-keV gamma ray is likely an $E2$ transition; the 1849-keV line is not, however, nor is it of the $E1$ type. These considerations result in $(9/2^-)$ and $(13/2^-)$ assignments for the states at 3519 and 4299 keV, respectively. A plausible scenario is that the 668- and 648-keV transitions below the 4299-keV state form a short dipole band, with the 3632- and 2984-keV levels being $(11/2^-)$ and $(9/2^-)$ members of the band, respectively, but without additional information this remains speculative.

The 4763-keV level decays to both positive- and negative-parity structures, specifically by a 775-keV transition to the 3988-keV $(17/2)^+$ state and a 463-keV transition to the 4299-keV $(13/2^-)$ state. The AC fits for the 775-keV transition are not consistent with either an $E2$ or $\Delta I = 0$ $E1$ assignment (Table IV). This restricts the likely spin and parity of the 4763-keV level to $(15/2^{\pm})$. It is somewhat surprising to find deexcitations towards states of both parities with comparable intensities, and with no observed feeding to any others of either parity. The possibility of there being a pair of degenerate states at 4763 keV can be discounted by the observation of the 986- and 1523-keV lines in coincidence gates following both decay paths. There is insufficient evidence to assign a parity to this state, but the spin can be tentatively given as (15/2).

VI. DISCUSSION

At low energies, the structure of ^{65,67}Cu is expected to be dominated by configurations involving the negative-parity $p_{3/2}$, $f_{5/2}$ and $p_{1/2}$ orbitals. As is the case in many nuclei of the region, at higher excitation energies $g_{9/2}$ particles can play a role, and excitations from the $f_{7/2}$ subshell, leading to proton two-particle one-hole ($2p1h$) configurations, are also possible. This situation presents a challenge to shell-model calculations as the dimensions for the full $fpg_{9/2}$ space are prohibitively large. In this situation, usually either the $f_{7/2}$ subshell is made available (with a Z or $N = 20$ core), but the $g_{9/2}$ orbital is excluded or, alternatively, the $f_{7/2}$ subshell is frozen with its full complement of eight nucleons (core of 28) and $g_{9/2}$ excitations are allowed. In the following subsections, results for ^{65,67}Cu are compared with the available systematics of the Cu isotopes, with known excitations in the corresponding

even-even Ni and Zn core nuclei, and with shell-model calculations in the $f_{5/2}pg_{9/2}$ valence space, in order to propose configuration assignments and to explore the implications of the necessary model-space truncations in the theory.

A. Negative-parity states

1. *Collective* $7/2^-$ *states*

The negative-parity states in ^{65}Cu identified in this work were all established in previous studies with no clear indication of a development into distinctive band structures. In contrast, one prominent strongly coupled band and two weak, shorter sequences emerge among the ^{67}Cu negative-parity states identified for the first time in the present study. Among the observed states in both nuclei are several $I^\pi = 7/2^-$ levels whose nature can be qualitatively investigated by examining the systematics of the Cu isotopes.

In Fig. 8, the energies of known $7/2^-$ levels below 3 MeV in odd-A $^{57-71}$Cu are plotted (similar to Fig. 7 in Ref. [39]). The dotted line marks those levels for which significant collectivity has been found, via a large $B(E2; 7/2^- \rightarrow 3/2^-)$ transition rate observed in Coulomb-excitation measurements [40] ($A = 63$ to 71) or deduced from the measured half-life and branching ratio to the ground state for the $7/2^-$ state ($A = 59$, 61) [50, 51]. The Cu levels are compared with the 2_1^+ energies of the corresponding even-A $^{56-70}$Ni cores, connected by a solid line in Fig. 8. (Note that a plot with a similar comparison, covering a slightly different range of Cu and Ni isotopes, was provided in Fig. 2 of Ref. [40].) These collective $7/2^-$ states, including those at 1482 keV in ^{65}Cu and 1669 keV in ^{67}Cu from the present work, are yrast over most of the plotted range of isotopes. These levels are found to follow the trend of the 2_1^+ states in their Ni core isotones quite closely, including a high excitation energy at magic $N = 28$, ^{57}Cu with an additional peak at a somewhat lesser value at $N = 40$, ^{69}Cu. This is consistent with those states in Cu having a dominant $\pi p_{3/2} \otimes 2^+$ configuration—i.e., they are associated with the weak coupling of a $p_{3/2}$ proton to the Ni core and they decay to the respective $[\pi p_{3/2} \otimes 0^+]_{3/2^-}$ ground states.

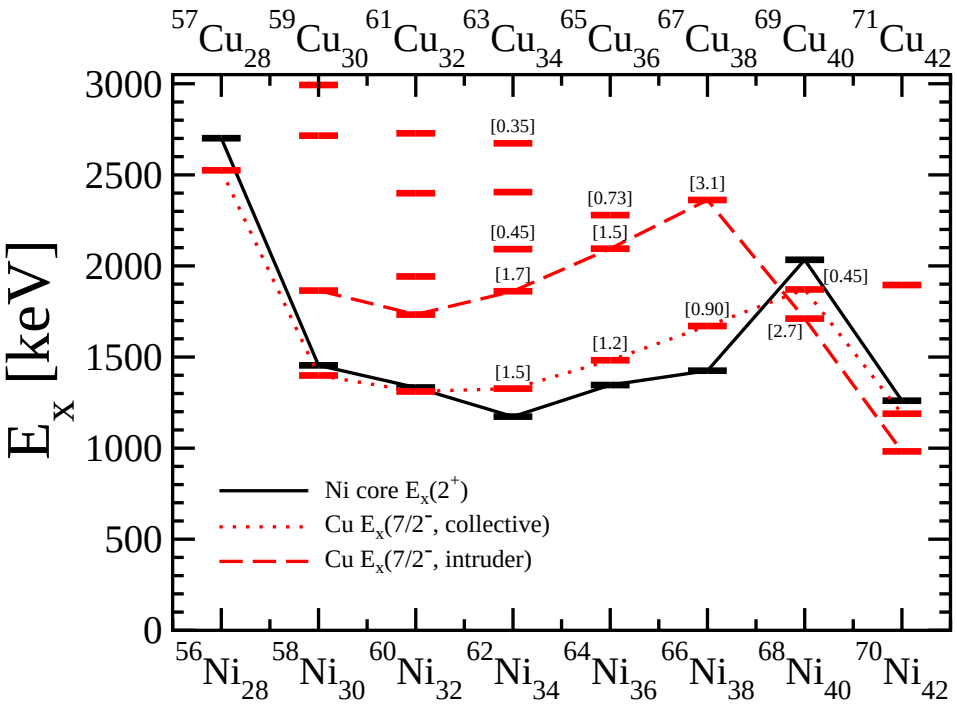

FIG. 8: (Color online) Excitation energies E_x of $7/2^-$ levels in the odd-A Cu isotopes compared with the 2_1^+ energies in the corresponding even-A Ni cores. The dotted (red) line connects $7/2^-$ states that have large $B(E2)$ strengths to the ground state, as described in the text. The dashed (red) line connects (and is extrapolated from) those found to have large spectroscopic factors in Zn(d,^{3}He) transfer [38]; the measured values are given in square brackets. Level energies for ^{65,67}Cu are from this work; Ni and the other Cu isotopes are from Refs. [47, 49–62].

2. *Single-particle intruder* $7/2^-$ *states*

The dashed line in Fig. 8 connects the $7/2^-$ states in the odd-$A = 63$ to 69 Cu isotopes with the largest spectroscopic strength for $f_{7/2}$ protons in Zn(d,^{3}He) reactions [38]. The values reported in Ref. [38] are indicated in square brackets in the figure. The line is extrapolated down to ^{59}Cu and up to ^{71}Cu. These states would correspond to those with the largest proton $2p1h$ contribution to their configuration, and involve the excitation of an $f_{7/2}$ proton across the $Z = 28$ shell gap.

The $7/2^-$ levels associated with the $f_{7/2}$ proton hole are found to be yrare in the mass range $A = 59$ to 67. They rise in energy as neutrons are added until, beyond $N = 38$, the energies drop rather rapidly. This decrease is usually associated with the occupation of $g_{9/2}$

neutron orbitals. Indeed, systematic energy shifts of single-particle levels are attributed to the tensor interaction: the increased occupation of $g_{9/2}$ neutrons in the heaviest Cu isotopes of Fig. 8 is expected to quench the $Z = 28$ shell gap because of the attractive $\pi f_{5/2} - \nu g_{9/2}$ and repulsive $\pi f_{7/2} - \nu g_{9/2}$ interactions. Consequently, the energy required to excite an $f_{7/2}$ proton across to the $p_{3/2}$ or $f_{5/2}$ orbital is reduced [41]. An alternative or complementary explanation that needs to be considered consists of the occupation of low-Ω $g_{9/2}$ neutron orbitals driving the nuclear shape towards prolate deformation, with the occupation of the high-Ω $f_{7/2}$ proton hole enhancing shape-driving effects. The resulting shell gap would again be smaller, rendering the $\pi f_{7/2}$ excitation energetically favorable. Note that Stefanescu *et al.* [40] concluded from $B(E2)$ data obtained in Coulomb-excitation measurements in odd-A $^{67-73}$Cu that there was no indication of shell quenching. However, the $\pi f_{7/2}^{-1}$ states under discussion here were not populated in Ref. [40] and their occupation could still have a strong polarizing effect on the nucleus.

In several of the odd-A Cu isotopes, the aforementioned $7/2^-$ states are the bandheads of cascades of fairly regular $M1/E2$ transitions with $E2$ crossovers. Specifically, a band in ^{59}Cu attributed to the $\pi f_{7/2}^{-1}$ configuration was identified in Ref. [42] and subsequently extended in Ref. [43] to $I^\pi = 23/2^-$; a band built on the 2361-keV $7/2^-$ state and reaching $I^\pi = (15/2^-)$ in ^{67}Cu is new to the current work (see Fig. 5); and a $\pi f_{7/2}^{-1}$ band in ^{69}Cu extending up to $13/2^{(-)}$ was observed in Ref. [44].

In ^{61}Cu, there is no single distinctive sequence of dipole transitions that can readily be associated with the $\pi f_{7/2}^{-1}$ state; the presence of one or more additional nearby negative-parity states for most spins in the 7/2 to 17/2 range, with "crosstalk" between the levels, results in a more complex picture [45]. There is currently even less evidence for such a band in ^{63}Cu [46, 47]. In ^{65}Cu, possible candidate members of a $\pi f_{7/2}^{-1}$ band are the 2094-keV $7/2^-$, 2406-keV $(7/2, 9/2)^-$, and 2998-keV $11/2^-$ states connected by 312- and 592-keV $M1/E2$ transitions with no observed $E2$ crossover gamma ray (Fig. 2); this sequence lacks the regularity of those found in ^{59,67,69}Cu. Finally, ^{71}Cu was found to exhibit a short (two-gamma-ray) $M1/E2$ cascade, depopulating an $(11/2^-)$ level at 1974 keV and feeding the 981-keV $7/2^-$ state. The number of gamma rays observed in these bands gets smaller from ^{67}Cu to ^{69}Cu to ^{71}Cu, possibly due in part to the lowering of the $\pi p_{3/2}\nu[p_{1/2}^{-2} g_{9/2}^2]$ (^{69}Cu) and $\pi p_{3/2}\nu g_{9/2}^2$ (^{71}Cu) configurations which provide the gamma-ray flux with a decay path bypassing the higher-spin states of the $\pi f_{7/2}^{-1}$ band.

The preceding observations about the development of the $\pi f_{7/2}^{-1}$ bands in the odd-A Cu nuclei can be understood qualitatively by considering Fig. 8. For ^{59,67,69}Cu, where this band is well developed, the $7/2^-$ state based on the $\pi f_{7/2}^{-1}$ configuration (connected by the dashed line in the figure) is fairly well separated in energy from other known nearby $7/2^-$ states apart from, at most, a collective $7/2^-$ level. In the latter two nuclei, the bulk of the $f_{7/2}$ strength is found to be concentrated into a single state, as evidenced by the spectroscopic factors noted in square brackets in Fig. 8. In ^{61,63,65}Cu, several additional low-lying $7/2^-$ levels are present, and fragmentation occurs for the $f_{7/2}$ strength into a number of these in ^{63,65}Cu, as indicated by the smaller spectroscopic factors (see, for example, Ref. [48]). The $\pi f_{7/2}^{-1}$ configuration likely mixes with others, accounting for the absence of a more clearly developed band similar to those in ^{59,67,69}Cu.

3. Comparison with even-even cores

In Sec. VI A 1, the interpretation of the collective $7/2^-$ levels as resulting from the weak coupling of a $p_{3/2}$ proton to the core 2^+ states in Ni was provided. This picture can also be extended to other observed levels in the odd-A Cu isotopes. A prime example of this is ^{59}Cu, which is a fairly simple system with one proton and two neutrons outside a ^{56}Ni core. Figure 11 of Ref. [42] provides an illustration of the weak particle-core coupling in this nucleus, with the available single-particle proton orbitals near the Fermi surface manifesting their presence in observed sequences of states mimicking the neighboring even-even ^{58}Ni ground-state band. Specifically, groups of states with $I^\pi = \{3/2^-, 7/2^-, 11/2^-\}$, $\{5/2^-, 9/2^-, 13/2^-\}$, and $\{9/2^+, 13/2^+, 17/2^+\}$ could be interpreted as, respectively, a $p_{3/2}$, $f_{5/2}$, or $g_{9/2}$ proton weakly coupled to the $\{0^+, 2^+, 4^+\}$ members of the ^{58}Ni ground-state band. (The $f_{7/2}$ proton-hole sequence will be discussed separately below.)

Attempts to provide similar comparisons between ^{65,67}Cu and their corresponding Ni cores are met with less success than for ^{59}Cu. Although the yrast $7/2^-$ levels are fairly good matches for a $\pi p_{3/2} \otimes 2^+$ interpretation, as noted in Sec. VI A 1 and in Fig. 8, this cannot be extended to the coupling of the $p_{3/2}$ proton to the 4^+ state to result in an $11/2^-$ state. In ^{65}Cu, the sole $11/2^-$ candidate identified in this work is at 2998 keV and has been associated with the $\pi f_{7/2}^{-1}$ configuration (see Sec. VI A 2), although the configurations may be highly mixed; other $11/2^-$ states from the literature [17] are at too high an energy to correspond

to a simple $\pi p_{3/2} \otimes 4^+$ coupling [cf. $E_x(4^+) = 2610$ keV]. Similarly, only the 3431-keV $11/2^-$ level assigned to the $\pi f_{7/2}^{-1}$ configuration was observed in ^{67}Cu. Little can be said about the $\pi f_{5/2}$ sequences in ^{65,67}Cu: Only the $5/2^-$ state has been firmly identified in either nucleus. The one candidate for the $[\pi f_{5/2} \otimes 2^+]_{9/2^-}$ state in ^{65}Cu is at 2406 keV, again possibly mixing with the $\pi f_{7/2}^{-1}$ configuration, while in ^{67}Cu there is no likely candidate. The coupling of a $g_{9/2}$ proton to the core leads to positive-parity states which are discussed in Sec. VI B.

In Ref. [42], the $\pi f_{7/2}^{-1}$ band in ^{59}Cu was also compared to the ground-state band of ^{58}Ni with considerably poorer agreement than were the $\pi p_{3/2}$, $\pi f_{5/2}$, or $\pi g_{9/2}$ sequences. Arguably, such a comparison should instead be made with the ^{60}Zn ground-state band rather than ^{58}Ni since it involves a proton hole. As can be seen on the left side of Fig. 9, however, this does not represent an improvement—the $11/2^-$ and $15/2^-$ levels are, respectively, ∼450 and ∼850 keV higher in energy than the 2^+ and 4^+ states in ^{60}Zn to which the $f_{7/2}$ proton hole would presumably couple. Here, the so-called $\pi f_{7/2}^{-1}$ band thus appears to be of a more complex character than a simple weak coupling of a proton (hole) to the core. For example, the deformation-driving nature of the intruder orbital may play a significant role.

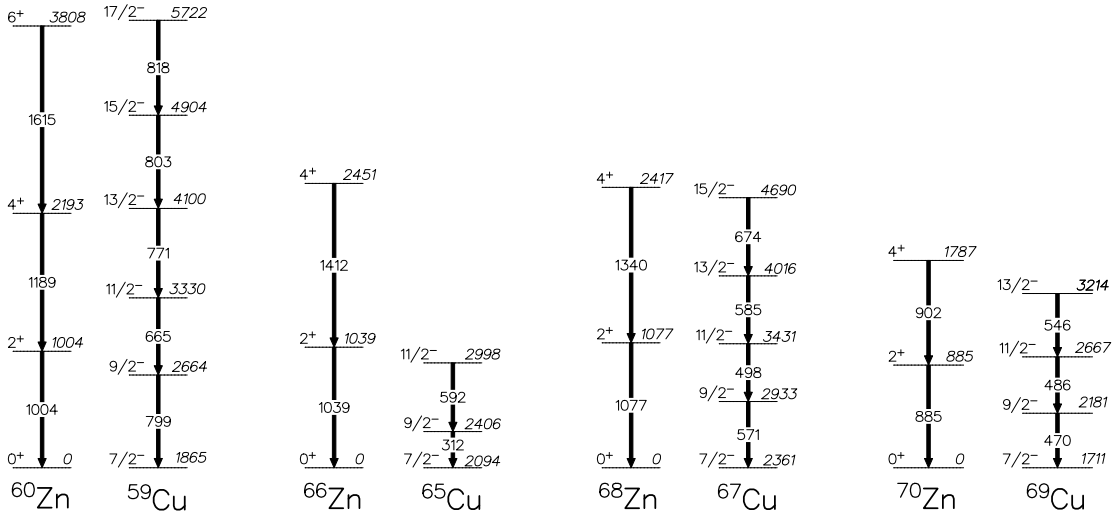

FIG. 9: Structures in odd-A Cu associated with $\pi f_{7/2}^{-1}$ configurations compared to the ground-state bands of their corresponding even-A Zn isotones. For the purposes of this comparison, the 2406-keV level in ^{65}Cu is assumed to have $I^\pi = 9/2^-$. Data are from this work for ^{65,67}Cu, Refs. [42, 50] and [44] for ^{59,69}Cu, and [56, 59–61] for ^{60,66,68,70}Zn.

Unlike the comparison between ^{59}Cu and the ^{60}Zn core, the $7/2^-$, $11/2^-$, and $15/2^-$

states of the $\pi f_{7/2}^{-1}$ sequence in ^{67}Cu match up rather well with the 0^+, 2^+, and 4^+ members of the ^{68}Zn ground-state band, as can be seen in Fig. 9. This may suggest that, for ^{67}Cu, the addition of the $f_{7/2}$ proton does not significantly alter the underlying structure of the sequence—i.e., it more closely resembles weak coupling to the core than its ^{59}Cu counterpart. Recent g-factor measurements in ^{68}Zn suggested the possible involvement of $\pi f_{7/2}$ particle-hole excitations for the 4^+ state [63, 64], although this result was disputed [65]; if true, the presence of the intruder orbital already in the Zn core might contribute to its similarity with the $\pi f_{7/2}^{-1}$ state in ^{67}Cu. In ^{65,69}Cu, the $11/2^- - 7/2^-$ spacings (904 and 956 keV, respectively) are also similar to the $2^+ - 0^+$ energy differences in ^{66,70}Zn (1039 and 885 keV); neither band extends as high as $15/2^-$, so no comparison can be made with the core 4^+ levels for these nuclides.

4. Nature of the $\pi f_{7/2}^{-1}$ sequences

As can be inferred from the preceding section, the nature of the $\pi f_{7/2}^{-1}$ sequences deserves closer scrutiny. A simple core-coupling approach seems inadequate. Juutinen *et al.* described the states in ^{59}Cu above the 1865-keV $7/2^-$ bandhead as being of vibrational character in their comparison with the ^{58}Ni ground-state band [42]. Andreoiu *et al.*, on the other hand, treated the same sequence instead as a rotational band and used Cranked Nilsson-Strutinsky calculations in their interpretation [43]. To help better understand these intruder bands in the Cu isotopes, which have one proton outside the $Z = 28$ closed shell, the structure of the $Z = 51$ Sb isotopes, outside the $Z = 50$ closed shell, can be considered for comparison. In odd-A $^{113-123}$Sb, strongly coupled band structures with $9/2^+$ bandheads were observed and attributed to an analogous excitation of $g_{9/2}$ protons across the $Z = 50$ shell gap [66]. Those deformation-driving excitations led to fairly regular rotational sequences of $M1/E2$ transitions with somewhat weaker $E2$ crossovers. The bands in ^{59,67,69}Cu also exhibit some degree of regularity in their gamma-ray sequences, which is suggestive of an interpretation as a collective rotational structure involving a high-Ω orbital that would drive the deformation and generate a sequence of dipole transitions. The moment of inertia ($\mathcal{J} = I/E_\gamma$) in these Cu nuclei is about half that of those found in the dipole bands in ^{115,117,119}Sb, suggesting smaller deformation induced by the $f_{7/2}$ intruder orbital compared to that of the $g_{9/2}$ proton.

A particle-core coupling model (PCM) was applied in Ref. [39] to describe quite satisfac-

torily the short $\pi f_{7/2}^{-1}$ sequences in ^{69,71}Cu (dubbed "quasi-bands" in [39]) mentioned above. The model involved coupling a particle or hole to the collective quadrupole and octupole vibrations of the corresponding even-even core, with the core assumed to be unchanged by the coupling. Data for the corresponding band in ^{67}Cu were unavailable prior to the present work; it would be interesting to determine if PCM calculations can also reproduce the observed $\pi f_{7/2}^{-1}$ band structure in this particular case.

5. Additional negative-parity structures

As mentioned in Sec. VI A 1, two short sequences in addition to the $\pi f_{7/2}^{-1}$ band emerge among the negative-parity states in ^{67}Cu. With limited information about the spins of the members of these sequences, any conclusion about them is speculative. (Negative parity is assumed because of their preferential feeding to only states of this parity.) No counterparts for these structures have been identified in ^{65}Cu.

6. Shell-model calculations

The spectra of states in ^{65,67}Cu were calculated with the shell-model code ANTOINE [67]. The valence space was restricted to the $f_{5/2}$, $p_{3/2}$, $p_{1/2}$, and $g_{9/2}$ orbitals for both protons and neutrons with a ^{56}Ni core. Calculations with both the JUN45 [6] and jj44b [68] effective interactions were performed. The former was fitted by Honma *et al.* [6] to experimental energies of 69 nuclei near $Z = 28$ or $N = 50$ with masses $A = 63 - 96$; the authors note that the Ni and Cu isotopes were specifically excluded from the fits because of the softness of the ^{56}Ni core due to expected significant excitations of the $f_{7/2}$ nucleons, which fall outside of the model space, from below the $Z = 28$ gap [6]. The jj44b interaction, on the other hand, incorporates experimental fit parameters primarily from $Z = 28 - 30$ nuclei and $N = 48 - 50$ nuclei [68].

The results of the calculations for negative-parity levels in ^{65,67}Cu are presented in Figs. 10 and 11, respectively, alongside the corresponding experimental data; positive-parity states will be discussed in Sec. VI B 2. For both the JUN45 and jj44b interactions, a specified number of the lowest-energy states with designated spin-parity quantum numbers are reported. These include one $1/2^-$, two $3/2^-$ and $5/2^-$, and three $7/2^-$ levels for both nuclei, as well

as one (three) $9/2^-$ and one (two) $11/2^-$ state in ^{65}Cu (^{67}Cu). For ^{67}Cu, the spectrum was further extended by two levels each with $I^\pi = 13/2^-$ and $15/2^-$, and a single $17/2^-$ state. This set covers the experimental range of spins observed in the current work as well as the $1/2^-_1$ and $3/2^-_2$ states in ^{65}Cu and the $(1/2)^-_1$, $3/2^-_2$, and $(5/2)^-_2$ states in ^{67}Cu taken from the literature [17, 47]. The 4763-keV state and those decaying to it in ^{67}Cu (see Fig. 5) are excluded from the figure because of the noted ambiguity of their parity assignments.

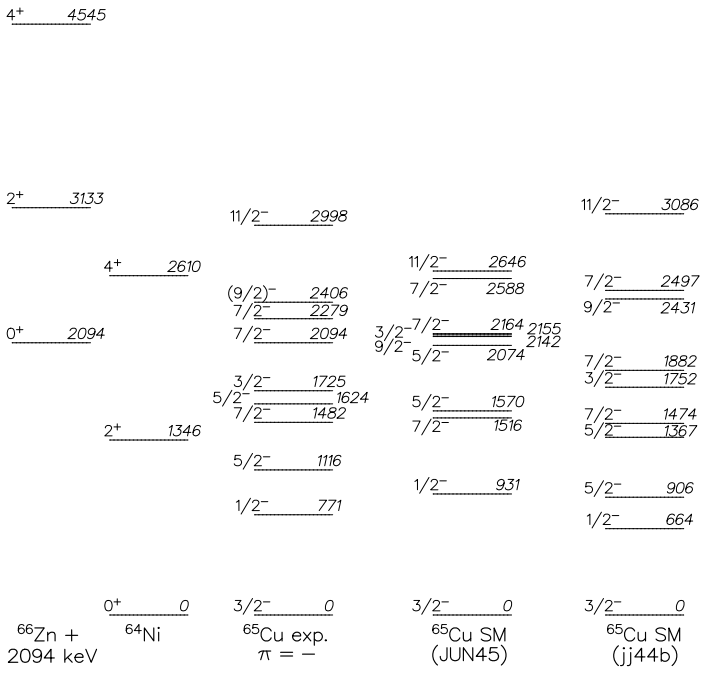

FIG. 10: Experimental negative-parity levels in ^{65}Cu compared to the ground-state bands of the even-even Ni [58] and Zn [59] isotones and shell-model calculations using the JUN45 and jj44b interactions (see text).

The ground states of both ^{65,67}Cu are determined to be associated with a $\pi p_{3/2}$ configuration. This is intuitively obvious, as the $p_{3/2}$ orbital is lowest in energy above the $Z = 28$ gap in this region. Details of the calculations for excited states in both nuclei are presented below.

a. ^{65}Cu The negative-parity spectrum of states calculated with the JUN45 interaction has several noteworthy deviations from the data for ^{65}Cu. The energies of both $5/2^-$ levels as well as that of the $3/2^-_2$ state are predicted to be over 400 keV higher than observed, whereas the calculated $11/2^-$ state is about 350 keV lower than found experimentally. Most of the remaining states in the JUN45 calculation are within 200 keV of the data. This

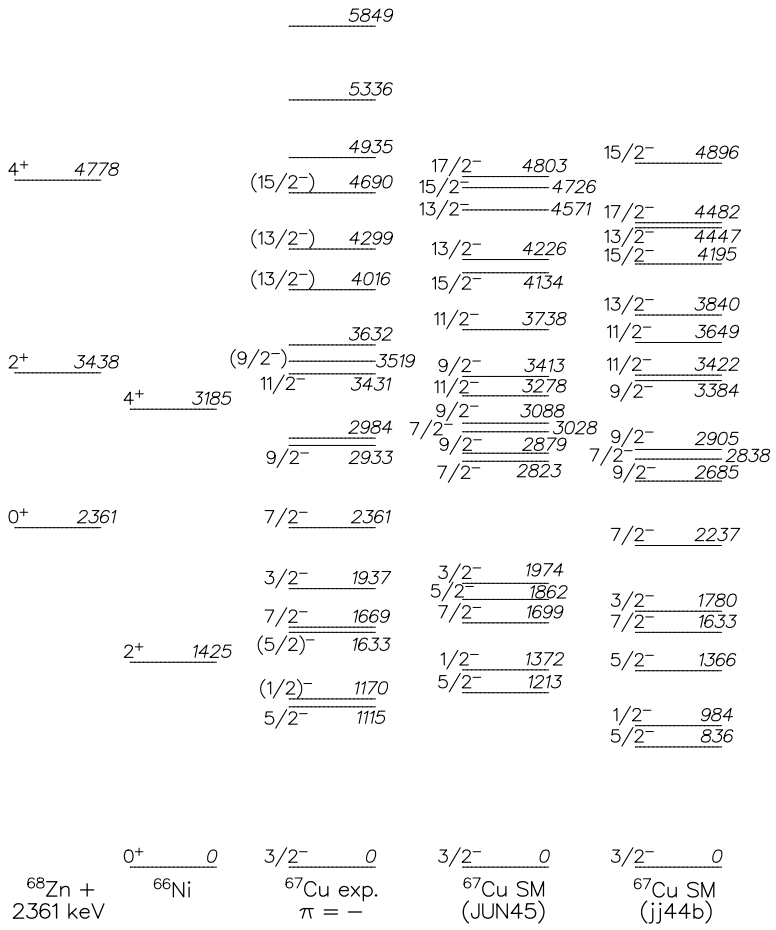

FIG. 11: Experimental negative-parity levels in ^{67}Cu compared to the ground-state bands of the even-even Ni [59] and Zn [60] isotones and shell-model calculations using the JUN45 and jj44b interactions (see text).

feature of the $5/2^-$ levels was already noted by Honma *et al.* [6] as being likely attributable to the absence of any possible excitations from the $f_{7/2}$ orbitals in the $f_{5/2}pg_{9/2}$ model space employed. Indeed, a comparison with GXPF1 calculations (which include the $f_{7/2}$ rather than the $g_{9/2}$ orbital) indicated that nearly half of the contributions to the wave function of the ^{65}Cu $5/2^-_1$ state involve $f_{7/2}$ excitations [6]. With JUN45, this state is found to have a mostly $\pi p_{3/2}$ configuration, as do all three $7/2^-$ states. The $5/2^-_2$ state, on the other hand, is predicted with JUN45 to have a dominant $\pi f_{5/2}$ configuration.

The results of the jj44b calculations are in considerably better agreement with the measured excitation energies in ^{65}Cu than are those using the JUN45 interaction. The ordering of the states is mostly reproduced, apart from an inversion of two closely spaced pairs, the

$5/2_2^-$ and $7/2_1^-$ levels and the $9/2_1^-$ and $7/2_3^-$ levels. The $5/2_{1,2}^-$ and $3/2_2^-$ levels that are problematic using the JUN45 interaction are far better described with jj44b, with the latter state predicted within 30 keV of the data. This improved agreement is not so surprising, since the jj44b interaction was obtained by including the Ni isotopes whose structure is known to be influenced by $\pi f_{7/2}$ excitations. The absence of this orbital from the model space requires that its influence be incorporated into the interactions involving the active $f_{5/2}$, $p_{3/2}$, $p_{1/2}$, and $g_{9/2}$ orbitals. Consequently, the calculations using these compensating interactions should be expected to work reasonably well near the $Z = 28$ closed shell. This is an approximation, however, to be used only until the option of performing calculations with the full $fpg_{9/2}$ valence space becomes more tractable. In the jj44b calculations, the nature of the two lowest $5/2^-$ states is reversed from that of JUN45; namely, the yrast $5/2^-$ level is found to be predominantly of $\pi f_{5/2}$ character while the yrare level is mostly of a $\pi p_{3/2}$ nature. With this in mind, a reinterpretation of the JUN45 results is that the 1570-keV calculated $5/2_1^-$ state may actually correspond to the *second* experimental $5/2^-$ state at 1624 keV, with both the JUN45 and jj44b interactions predicting a $\pi p_{3/2}$ configuration and reproducing the measured energy rather well. It is then the $\pi f_{5/2}$, $5/2^-$ level that is nearly 1 MeV too high in the JUN45 calculations, at 2074 compared to 1116 keV, suggesting that this level is very strongly influenced by the $\pi f_{7/2}$ orbital that is absent from these calculations.

The jj44b and JUN45 interactions agree on the dominant $\pi p_{3/2}$ configurations for the two lowest $7/2^-$ states, but the former instead ascribes the $\pi f_{5/2}$ configuration to the $7/2_3^-$ state. Again, the calculations for these $7/2^-$ levels must compensate for the missing $f_{7/2}$ orbital. Finally, the experimental $9/2^-$ and $11/2^-$ states are well reproduced by the jj44b calculations.

b. ^{67}Cu For ^{67}Cu, both the JUN45 and jj44b interactions correctly predict the set of states observed below 2 MeV and, in the case of jj44b, also with the proper ordering. The deviation for the $5/2^-$ energies for the JUN45 interaction is seemingly not as severe here as was found for ^{65}Cu. In fact, the agreement with the data is better with JUN45 than jj44b for those levels. However, based on the same argument provided above for ^{65}Cu, the predicted nature of the two $5/2^-$ levels is reversed for the JUN45 interaction compared to jj44b, such that the $\pi f_{5/2}$, $5/2^-$ level is pushed up rather high in energy to 1862 keV (compared to the experimental value of 1115 keV) while the $\pi p_{3/2}$ $5/2^-$ level is about 400 keV lower than the measured 1633-keV $(5/2)^-$. For jj44b, both $5/2^-$ levels are about 270 keV below the

corresponding observed ones.

Three $7/2^-$ states were calculated with both the JUN45 and jj44b interactions for ^{67}Cu, while only two have been identified experimentally at 1669 and 2361 keV. Both sets of calculations predict a predominantly $\pi p_{3/2}$ $7/2^-$ level close in energy to the observed yrast state. The second $7/2^-$ level is reasonably well reproduced by the jj44b calculations, with a $\pi f_{5/2}$ configuration. In the JUN45 calculations, the lowest $7/2^-$ level with any sizable $\pi f_{5/2}$ component is pushed up to 3028 keV, which is about 670 keV above the measured $7/2^-_2$ energy. This result is expected, as the 2361-keV observed state was shown in Sec. VI A 2 to be due to the $\pi f^{-1}_{7/2}$ excitation, lying outside the current model space, which cannot be described with JUN45 and is approximated by the fitted jj44b interaction. Both sets of calculations predict a $7/2^-_3$ level around 2.8 MeV, based primarily on a $\pi p_{3/2}$ configuration, that has not been identified in the data.

Without definitive spin assignments for all of the (presumed) negative-parity states above 2.5 MeV in ^{67}Cu, a detailed comparison with the shell-model calculations becomes less straightforward. The 2933-keV $9/2^-$, 3431-keV $11/2^-$, and 4016-keV $(13/2^-)$ members of the band built upon the $\pi f^{-1}_{7/2}$ state at 2361 keV each have a theoretical counterpart that lies within $\sim$200 keV. (Note that, in some cases, there are two calculated levels located nearby in energy.) The 4690-keV $(15/2^-)$ state is not as well reproduced, with a $\sim$500-keV underestimation in both calculations. The improved agreement for the $9/2^-$, $11/2^-$, and $13/2^-$ states in this sequence in the JUN45 calculations compared to the large discrepancy found for the $7/2^-_2$ bandhead could be an indication that the $f_{7/2}$ hole becomes a less important contributor to the wave functions for these higher-spin states; put another way, there could be a sizable admixture of additional configurations formed without requiring the $f_{7/2}$ orbital, which are successfully calculable within the JUN45 model space.

Among the cluster of states to the left side of the level scheme in Fig. 5, the two at 2984 and 3632 keV have no I^π assignments and those at 3519 and 4299 keV are tentatively assigned $(9/2^-)$ and $(13/2^-)$, respectively. Considering the levels in the calculations that have not yet been associated with observed ones, the 2984-keV state could correspond to either $I^\pi = 7/2^-_3$ or $9/2^-_2$. If the former, then the calculated $9/2^-_2$ levels are $\sim$400 (JUN45) to 600 (jj44b) keV below what would be the experimental $(9/2^-_2)$ state at 3519 keV. If the latter, then the experimental $7/2^-_3$ level is still unobserved, and the 3519-keV state corresponds instead to a $(9/2^-_3)$ level, in agreement with both sets of calculations. The most

likely assignment for the 3632-keV state, based on the predicted energies, would be $11/2^-$. Recall that, in Sec. V B, it was suggested that the 3632- and 2984-keV levels are members of a dipole band with $I^\pi = (11/2^-)$ and $(9/2^-)$, respectively; these are consistent with the shell-model comparisons. No assignments have been attempted for the 4935-, 5336-, and 5849-keV states.

c. Summary of the shell-model calculations Despite the absence of the $f_{7/2}$ orbital in the shell-model valence space, the negative-parity spectra of states in ^{65,67}Cu are, to an extent, at least qualitatively reproduced by the calculations, with the jj44b interaction providing better overall agreement with the experimental level energies. However, these results indicate that, in order to obtain a more complete understanding of the nature of these levels, the proton $f_{7/2}$ hole is a necessary ingredient. The jj44b interaction is an approximation that circumvents this necessity somewhat, but consequently "disguises" the underlying structure for some of the observed states. Since the jj44b interaction is locally fitted for nuclei near the $Z = 28$ and $N = 50$ closed shells, it is understandably better suited to reproducing the Cu nuclei, while JUN45 is expected to have broader scope throughout the fpg shell. Interestingly, however, JUN45 appeared to be in better agreement with the data than jj44b for the $Z = 28$ nucleus ^{67}Ni in Ref. [69].

The calculations for ^{65,67}Cu using either set of interactions indicate that the $g_{9/2}$ neutron is needed for the description of the negative-parity levels, as configurations involving this orbital typically have a 20% or larger contribution to the wave functions. The need to include $f_{7/2}$ *neutron* orbitals for these nuclei cannot be determined from these results, but their contribution is likely small since the neutron Fermi level is in the upper fp shell and should be sufficiently far removed from the $N = 28$ shell gap. The proton $g_{9/2}$ orbital is found to have negligible influence on the negative-parity levels. One might then argue that calculations with a ^{48}Ca core, using the full fp space for protons and the $f_{5/2}pg_{9/2}$ space for neutrons, would be adequate for describing these nuclei. As will be demonstrated in the following section, however, this is insufficient for calculations of the positive-parity spectrum of states.

B. Positive-parity states

The level schemes of ^{65,67}Cu include similar positive-parity structures, with spins ranging from 9/2 to 17/2 with additional gamma-ray sequences feeding into the $15/2^+$ and $17/2^+$ levels (see Figs. 2 and 5). The odd-A Cu isotopes exhibit remarkable stability for the energy of the lowest $9/2^+$ state, located near 2.5 MeV, showing a variation of less than 100 keV from $A = 63$ to 71. Measurements of the spectroscopic factors indicate that there is a large $\pi g_{9/2}$ component for the yrast $9/2^+$ levels in ^{59,61,63,65}Cu (see, for example, the (^{3}He, d) work by Britton and Watson [30]). In the cases of ^{65,67,69}Cu, the $9/2^+$ level is found to decay to several negative-parity states, including direct feeding of the $3/2^-$ ground state via an $E3$ transition. The latter decay would correspond to a proton moving from a $g_{9/2}$ to a $p_{3/2}$ orbital. An $M2$ transition, several times weaker than the $E3$ gamma ray, is also found to depopulate the $9/2^+$ to the 1115-keV $5/2^-$ state in ^{67}Cu, but the corresponding transitions have not been identified in ^{65,69}Cu. Notably, the $E3$ decay carries a substantially larger fraction of the total $9/2^+$ level intensity in ^{67}Cu than in the other two nuclei; if the possible $M2$ transitions are proportionally weaker in ^{65,69}Cu, it is not surprising they remain unobserved. The difference in $E3$ intensities in ^{67}Cu compared to ^{65,69}Cu may be a reflection of the number of $7/2^-$ states to which the $9/2^+$ state can decay. In other words, the decays in ^{65,69}Cu are more likely to proceed via the multiple available $E1$ transitions than by the higher-multipolarity gamma rays.

In this section, the positive-parity states in ^{65,67}Cu are compared with their corresponding core nuclei and with shell-model calculations.

1. Comparison with even-even cores

All positive-parity states in the odd-A Cu isotopes of interest must arise from excitations of an odd number of nucleons into positive-parity $g_{9/2}$ orbitals. The interpretation of positive-parity states in ^{59}Cu as resulting from the weak coupling of a $g_{9/2}$ proton to the ^{58}Ni core was discussed in Sec. VI A 3. The stability of the yrast $9/2^+$ states over a range of isotopes and their large measured spectroscopic factors support a similar interpretation for the heavier nuclides. Treating this state in each odd-A Cu isotope as arising from a $\pi g_{9/2} \otimes 0^+$ coupling to the ground state of the even-A Ni core, by simple extension one might expect to find

similar couplings to higher-spin states, such as $\pi g_{9/2} \otimes \{2^+, 4^+\}$ to give $\{13/2^+, 17/2^+\}$, as was found in ^{59}Cu. An alternative scenario for generating positive-parity states, however, would be for the lower-energy $p_{3/2}$ proton to couple to negative-parity states in the Ni core which are interpreted as involving a $g_{9/2}$ *neutron* and either $\nu p_{1/2}$, $\nu p_{3/2}$, or $\nu f_{5/2}$ orbitals. For example, a $\pi p_{3/2} \otimes 5^-$ coupling would also lead to a $13/2^+$ state in Cu. Figure 12 compares the $13/2_1^+ - 9/2_1^+$ and, where known, $13/2_2^+ - 9/2_1^+$ excitation-energy differences in several odd-A Cu isotopes to the 2_1^+ energies of the corresponding Ni cores. Also shown are the excitation energies of the Ni 5^- states, less reference energies taken from their isotonic Cu $9/2^+$ states. (Although we are interested in comparing the excitation energies of the Ni 5^- and Cu $13/2^+$ states relative to their respective ground states [$E_x(5^-) - E_x(0^+)$ for Ni, $E_x(p_{3/2} \otimes 5^-) - E_x(p_{3/2} \otimes 0^+)$ for Cu], we subtract the common reference E_x(Cu $9/2^+$) from both so they can be compared on the same scale as the Ni $E_x(2^+)$ energies.) The two sets of $13/2^+$ states follow rather clear trends: One, yrast for the lighter isotopes and becoming yrare by ^{65}Cu, tracks with the 2^+ Ni core energies (apart from a deviation for ^{63}Cu); the other, yrare at ^{61}Cu, but rapidly decreasing in energy to become yrast for the heavier isotopes, follows quite closely the Ni 5^- systematics. A comparison of the $15/2^+$ and $17/2^+$ Cu energies with those of the 6^- and 7^- in Ni reveals similar trends. This leads naturally to the conclusion that, as neutrons are added to the Cu nuclei, the $\nu g_{9/2}$ orbital plays an increasing role in the positive-parity structures, bringing down their energies. Such behavior has also been demonstrated recently in neutron-rich Fe and Mn nuclides [23, 24].

This systematic effect is demonstrated in a different way in Fig. 13, where the excitation energies of the $9/2^+$ to $17/2^+$ states in the odd-A Cu isotopes from $A = 59$ to 69 are plotted with no reference energy subtracted. The contrast between the behavior of the $9/2_1^+$ state (nearly flat as a function of A for ^{63}Cu and above) and the rest of the positive-parity levels (rapidly decreasing with A) is clear. This highlights the difference between a configuration of $\pi g_{9/2}$ coupled to positive-parity core states for the former and $\pi p_{3/2}$ coupled to negative-parity core states (which necessarily involve the $\nu g_{9/2}$ orbital) for the latter. Plotting the negative-parity states in ^{64,66}Ni alongside the positive-parity states in ^{65,67}Cu in Figs. 14 and 15, respectively, the close correspondence (similar excitation energies) for 5^- and $[\pi p_{3/2} \otimes 5^-]_{13/2^+}$, 6^- and $[\pi p_{3/2} \otimes 6^-]_{15/2^+}$, and 7^- and $[\pi p_{3/2} \otimes 7^-]_{17/2^+}$ is apparent. One would expect to also observe a $9/2_2^+$ state, originating from the coupling of the $\pi p_{3/2}$ orbital to the 3^- of the core, which would similarly dive down in energy as A increases; a second

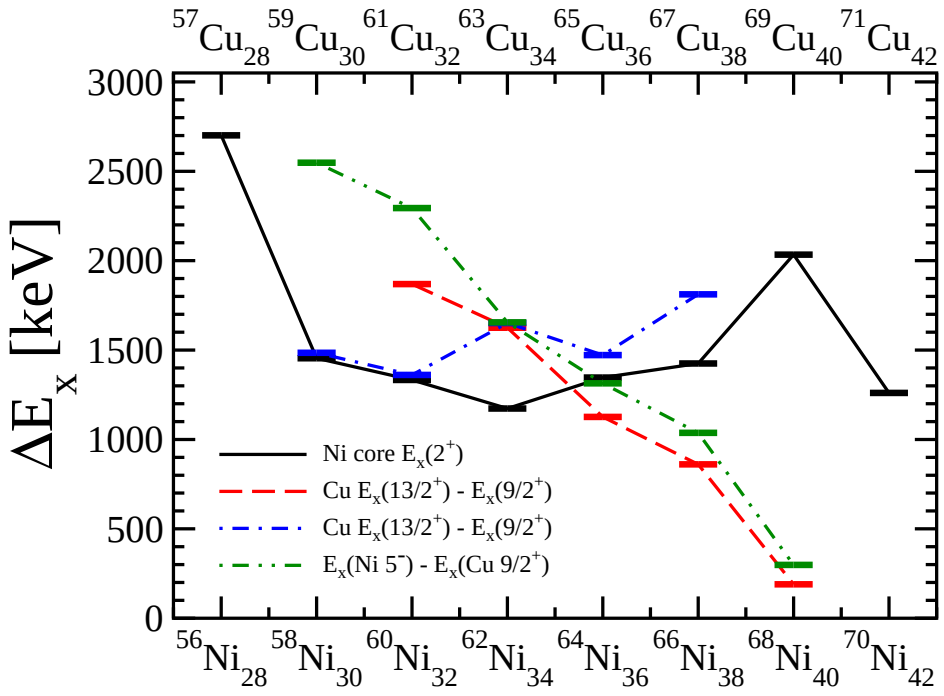

FIG. 12: (Color online) Energy differences between the $13/2^+_{1,2}$ and $9/2^+_1$ states in Cu [dashed (red) and dot-dashed (blue) lines] compared to energies of the 2^+_1 (solid black line) and 5^- levels [dash-double-dotted (green) line] in the Ni isotopes. The latter have a reference energy subtracted—see text for details. The $13/2^+_2$ state in ^{67}Cu is taken from Ref. [28]; results for ^{65,67}Cu are otherwise from the present work. Data for Ni and the other Cu isotopes are from Refs. [47, 49–62].

$9/2^+$ has not been systematically observed along this chain of Cu isotopes, however, so this expectation has not been experimentally confirmed. Honma *et al.* attribute the lowering of the $9/2^+$ ($\nu g_{9/2}$) state in the odd-A, neutron-rich Ni, Zn, and Ge isotopes to the $T = 1$ monopole interaction between the $\nu g_{9/2}$ and $\nu f_{5/2}$ orbitals as the latter is increasingly filled [6]. This would presumably apply also to the negative-parity states that involve the $\nu g_{9/2}$ orbital in even-A Ni isotopes and, by coupling to a $p_{3/2}$ proton, positive-parity states in the odd-A Cu isotopes as well.

The position of the $13/2^+_1$ level in ^{63}Cu is a noteworthy anomaly. Of the known states plotted in Fig. 12, it is the only one that deviates significantly from the systematics. As the two $13/2^+$ levels approach each other with changing neutron number, one would expect a repulsion between two levels with the same spin and parity quantum numbers, yet they appear here to be drawn closer together, differing by only 25 keV. This could suggest that

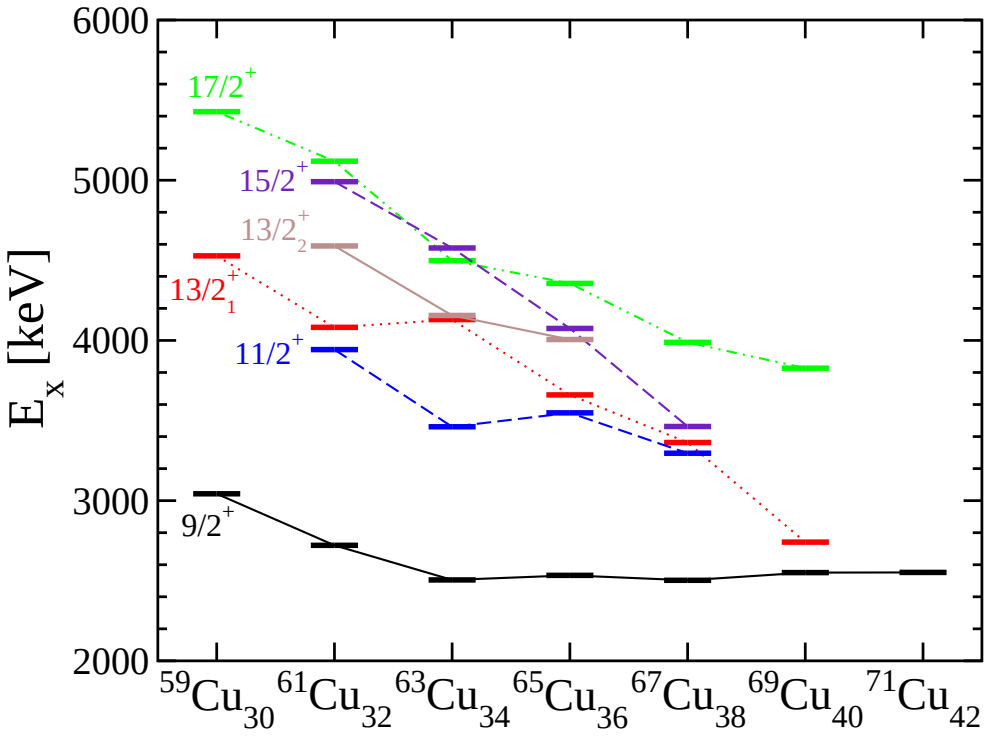

FIG. 13: (Color online) Excitation energies of positive-parity levels in odd-A Cu isotopes [42, 44, 45, 70, 71]. The 2551-keV level in ^{71}Cu is given as $(7/2^+)$ in the beta-decay work of Ref. [71]; however, an $I^\pi = 9/2^+$ assignment is also consistent with the observed beta feeding [71], as well as the energy and the decay pattern ($M2$ to $5/2^-$) of the $9/2^+$ states in the lighter isotopes, so the latter assignment is used here.

one of the spin assignments is incorrect, or that some other effect is influencing the $13/2^+_1$ energy. Either way, it is deserving of further investigation.

2. *Shell-model calculations*

Shell-model calculations were performed as described in Sec. VI A 6 for the positive-parity levels in ^{65,67}Cu; the results are presented in Figs. 14 and 15, respectively. Only the calculated states with the lowest energies are reported. For those with $I^\pi = 9/2^+$, $11/2^+$, $13/2^+$, $15/2^+$, and $17/2^+$, the two lowest computed states are given, while only one is reported for $I^\pi = 19/2^+$ and $21/2^+$.

The $9/2^+_1$ level in the JUN45 calculations is more than 500 keV too high in excitation energy in either nucleus. The underlying wave functions for these states are predicted with

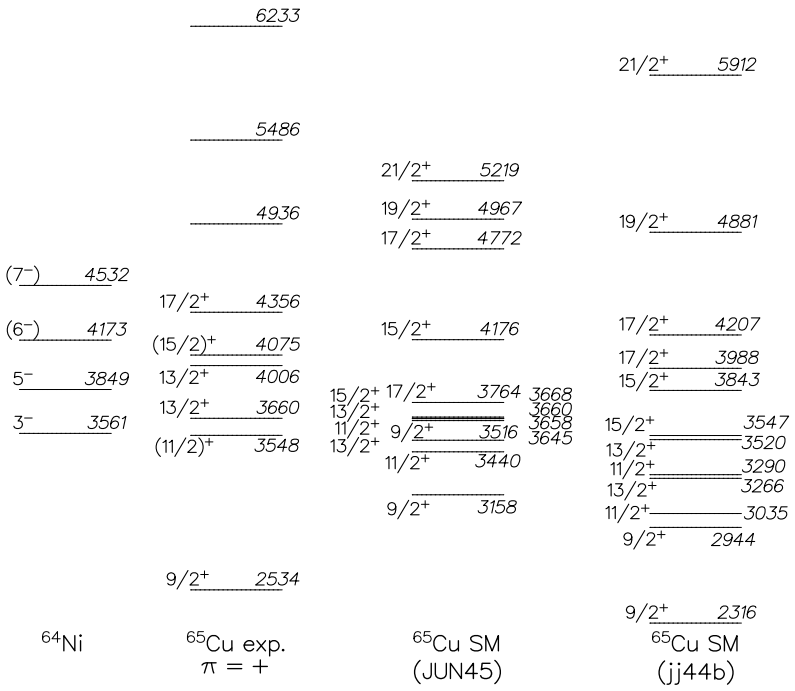

FIG. 14: Experimental positive-parity levels in ^{65}Cu compared to negative-parity states in the even-even Ni [58, 72] isotone and to shell-model calculations using the JUN45 and jj44b interactions (see text).

JUN45 to be dominated by $\pi p_{3/2}$ configurations, with only small components involving the $\pi g_{9/2}$ orbital. This is contrary to the systematically large $g_{9/2}$ spectroscopic strength deduced in $(^3\mathrm{He}, d)$ transfer studies for the $9/2^+$ states in the Cu isotopes with $A = 59$ to 65 [30]. Similar JUN45 calculations for ^{59}Cu, on the other hand, *do* indicate a large ($\sim$60%) $\pi g_{9/2}$ component in the wave function of the yrast $9/2^+$ state in that nucleus. Using the jj44b interaction, the calculated configurations for the $9/2^+$ levels in ^{65,67}Cu are grouped into approximately equal $\pi p_{3/2}$ and $\pi g_{9/2}$ contributions, and are found to result in a lowering of the excitation energies to over 200 keV below the experimental energies. This indicates that the role of the $g_{9/2}$ proton is not yet well understood in calculations for Cu nuclei in the more neutron-rich region.

The higher-lying positive-parity levels in both nuclei are predicted to be clustered rather closely together in the JUN45 and, to a lesser extent, in the jj44b calculations. All but one of these are found to have at most a $\pi g_{9/2}$ contribution of a few percent in the wave function, with the $\pi p_{3/2}$ orbital instead being dominant. (The anomaly is the $13/2^+_2$ level in

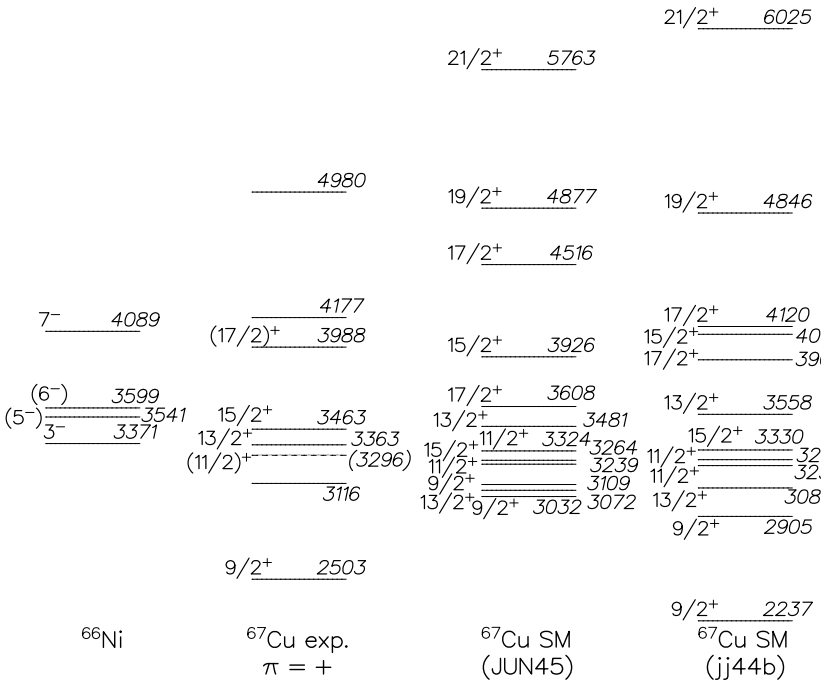

FIG. 15: Experimental positive-parity levels in ^{67}Cu compared to negative-parity states in the even-even Ni [59, 72] isotone and to shell-model calculations using the JUN45 and jj44b interactions (see text).

^{65}Cu, which only the jj44b calculations predict to be composed of ∼25% $\pi g_{9/2}$ components.) In the absence of an occupied $\pi g_{9/2}$ orbital in the odd-A Cu isotopes, positive-parity states must then arise from the occupation of an odd number of $g_{9/2}$ neutrons. Experimentally, the systematics, as shown in Figs. 12 and 13, lead to the same conclusion: apart from the $9/2^+_1$ state, the positive-parity levels in the Cu isotopes behave like the yrast negative-parity levels in their corresponding Ni core isotones which are attributed to configurations involving the $\nu g_{9/2}$ orbital.

In ^{65}Cu, the JUN45 spectrum of states is too compressed; that using the jj44b interaction is more appropriately spaced, but predicted ∼400-500 keV too low in energy. The agreement is better for ^{67}Cu with either set of interactions. There is sufficient qualitative agreement to propose tentative spin assignments for several states for which experimental data were inconclusive. The 4936-keV state in ^{65}Cu is close to the $19/2^+$ level predicted around 4.9 MeV in both calculations; however, the AD of the 862-keV transition to the $(15/2)^+$ 4075-keV state is inconsistent with an $E2$ multipolarity. Considering that the lower-spin

positive-parity levels in the jj44b calculations are all predicted hundreds of keV too low, the 4936-, 5486-, and 6233-keV experimental states could correspond to the 4207-keV $17/2_2^+$, 4881-keV $19/2_1^+$, and 5912-keV $21/2_1^+$ calculated levels, respectively.

There are three unassigned spins among the positive-parity states in ^{67}Cu, at 3116, 4177, and 4980 keV. The first of these could represent either the $9/2_2^+$ or the $13/2_1^+$ level. The former is a close match to both the JUN45 and jj44b predictions and is consistent with the observed intensity depopulating this state compared to the yrast $9/2^+$ level at 2503 keV. The latter assignment would address the fact that, in the calculations, the yrast $13/2^+$ state drops below the $11/2^+$, and the experimental $13/2^+$ state at 3363 keV would then match the calculated $13/2_2^+$ level instead. However, it would then be somewhat surprising to find strong decays only to the 3363-keV $13/2^+$ state. A $(9/2_2^+)$ assignment is preferred for the 3116-keV level. Based on the comparison between the experimental data and the jj44b calculations, the 4177-keV state may correspond to the predicted 4120-keV $17/2^+$ level, as both are $\sim$200 keV above the respective $17/2_1^+$ states. The 4980-keV state would then likely have $I^\pi = 19/2^+$ quantum numbers, since the lowest $21/2^+$ is predicted to be considerably higher in energy.

In Ref. [39], the authors conclude that $N = 40$ represents a significant subshell closure, arguing that the observation of the monopole shift of the $f_{5/2}$ and (possibly) $g_{9/2}$ proton orbitals only beyond $N = 40$ indicates a negligible $\nu g_{9/2}$ occupancy for $N < 40$. However, it is clear from the present study that the influence of the $g_{9/2}$ neutron manifests itself in the positive-parity levels at lower N, particularly in the higher-energy excitations. Even for the $3/2^-$ ground state, our calculations (with either interaction) indicate that about 30% of the wave-function components include one or more $g_{9/2}$ neutrons in $N = 36$ ^{65}Cu; this number rises to around 50% for $N = 38$ ^{67}Cu. Similar behavior was demonstrated for the neutron-rich Fe isotopes, with negative-parity levels involving the $g_{9/2}$ neutron orbital steadily decreasing in energy with increasing A and with a non-negligible calculated $\nu g_{9/2}$ contribution to the ground-state wave function upon reaching $N = 36$ ^{62}Fe [23]. The importance of multiparticle-multihole excitations in the configurations involving the $g_{9/2}$ neutron orbital has also been highlighted in recent spectroscopy of yrast and near-yrast states in ^{67}Ni [69].

a. Summary of the shell-model calculations Overall, the observed positive-parity levels for ^{65,67}Cu can be described better in terms of the weak coupling of a $p_{3/2}$ proton to the

negative-parity states of the ^{64,66}Ni cores than with shell-model calculations using the currently available JUN45 and jj44b effective interactions. The summary of Sec. VI A 6 alluded to the inadequacy of using strictly the fp valence space for describing the proton system in these nuclei. Here, it is apparent that both $g_{9/2}$ protons and neutrons are necessary in the calculations for the positive-parity states, just as $f_{7/2}$ proton holes are important to those with negative parity. Thus, the full $fpg_{9/2}$ valence space is needed in order to calculate a complete spectrum of states with both parities.

VII. CONCLUSIONS

The level schemes of ^{65,67}Cu have been extended in a study of (deep-)inelastic reactions with Gammasphere. Positive-parity structures have been observed up to at least $I^\pi = 17/2^+$ in both nuclei. In ^{67}Cu, a strongly coupled band and two additional structures were also identified for the first time among the negative-parity states. A comparison of the experimental levels in ^{65,67}Cu with systematics of the odd-A Cu and neighboring even-A Ni and Zn nuclides provides a consistent interpretation for a number of the observed levels. Weak coupling of a $p_{3/2}$ proton to the ground and 2_1^+ states and to negative-parity configurations in the adjacent Ni core nuclei manifests itself as, respectively, the $3/2^-$ ground, the $7/2_1^-$, and several positive-parity states identified in both ^{65,67}Cu. The $7/2_2^-$ state in ^{67}Cu is established as the bandhead of an intruder $\pi f_{7/2}^{-1}$ configuration; a counterpart to this structure was not found to develop in ^{65}Cu, possibly due to significant fragmentation of the $f_{7/2}$ single-particle strength over several $7/2^-$ levels in that nucleus. In the positive-parity structures, competition is seen between configurations involving $g_{9/2}$ protons and those with $g_{9/2}$ neutrons. The yrast $9/2^+$ states are likely attributable to the former and vary little in excitation energy across the odd-A $^{63-71}$Cu isotope chain, whereas the latter decrease rapidly in energy with increasing mass as $N = 40$ is approached. These results demonstrate the importance of including both the $f_{7/2}$ and $g_{9/2}$ orbitals in the shell-model calculations. With the additional data provided in the current work and inclusion of the full $fpg_{9/2}$ proton and neutron valence spaces, it is expected that an improved set of two-body matrix elements could be obtained for the description of nuclei in this region.

Acknowledgments

The authors thank J. P. Greene (ANL) for target preparation. This work was supported in part by the U.S. Department of Energy, Office of Nuclear Physics, under Grant No. DE-FG02-94-ER40834 and Contract No. DE-AC02-06CH11357, and by the Polish Ministry of Science under Contract Nos. 1P03B05929 and NN202103333. EGJ was a participant in the Department of Energy's Science Undergraduate Laboratory Internships Program through the ANL Division of Educational Programs.

---

[1] J. P. Schiffer *et al.,* Phys. Rev. Lett. **108**, 022501 (2012).

[2] K. T. Flanagan *et al.*, Phys. Rev. Lett. **103**, 142501 (2009).

[3] V. Golovko *et al.*, Phys. Rev. C **70**, 014312 (2004).

[4] M. Honma, T. Otsuka, B. A. Brown, and T. Mizusaki, Phys. Rev. C **69**, 034335 (2004).

[5] M. Honma, T. Otsuka, B. A. Brown, and T. Mizusaki, Eur. Phys. J. A **25**, s01, 499 (2005).

[6] M. Honma, T. Otsuka, T. Mizusaki, and M. Hjorth-Jensen, Phys. Rev. C **80**, 064323 (2009).

[7] P. Vingerhoets *et al.*, Phys. Lett. B **703**, 34 (2011); Advances in Radioactive Isotope Science conference, Leuven, poster #406 (2011) [https://iks32.fys.kuleuven.be/indico/getFile.py/access?contribId=407&sessionId=4&resId=0&materialId=poster&confId=0].

[8] J. Rikovska *et al.*, Phys. Rev. Lett. **85**, 1392 (2000).

[9] T. E. Cocolios *et al.*, Phys. Rev. Lett. **103**, 102501 (2009).

[10] P. Vingerhoets *et al.*, Phys. Rev. C **82**, 064311 (2010).

[11] J. K. Dickens, Nucl. Phys. **A401**, 189 (1983).

[12] Yu. G. Kosyak *et al.*, Bull. Rus. Acad. Sci. Phys. **64**, 321 (2000).

[13] C. P. Swann, Phys. Rev. C **13**, 1104 (1976).

[14] M. Giannini, P. Oliva, D. Prosperi, and G. Toumbev, Nucl. Phys. **A101**, 145 (1967).

[15] B. Y. Guzhovskii, I. M. Borkin, A. G. Zvenigorodskii, V. S. Rudnev, A. P. Solodovnikov, and S. V. Trusillo, Bull. Acad. Sci. USSR Phys. Ser. **33**, 119 (1970).

[16] G. Mairle, M. Seeger, M. Ermer, P. Grabmayr, A. Mondry, and G. J. Wagner, Phys. Rev. C **47**, 2113 (1993).

[17] E. Browne and J. K. Tuli, Nucl. Data Sheets **111**, 2425 (2010).

[18] M. Asai, T. Ishii, A. Makishima, I. Hossain, M. Ogawa, and S. Ichikawa, Phys. Rev. C **62**, 054313 (2000).

[19] I. Y. Lee, Nucl. Phys. **A520**, 641c (1990).

[20] N. Hoteling *et al.*, Phys. Rev. C **74**, 064313 (2006).

[21] N. Hoteling *et al.*, Phys. Rev. C **77**, 044314 (2008).

[22] I. Stefanescu *et al.*, Phys. Rev. C **79**, 034319 (2009).

[23] N. Hoteling *et al.*, Phys. Rev. C **82**, 044305 (2010).

[24] C. J. Chiara *et al.*, Phys. Rev. C **82**, 054313 (2010).

[25] D. C. Radford, Nucl. Instrum. Methods Phys. Res. A **361**, 297 (1995).

[26] S. Zhu *et al.* (unpublished).

[27] K. Starosta, D. B. Fossan, T. Koike, C. Vaman, D. C. Radford, and C. J. Chiara, Nucl. Instrum. Methods Phys. Res. A **515**, 771 (2003).

[28] K. Nybø, H. Helstrup, T. F. Thorsteinsen, and G. Løvhøiden, Phys. Scr. **63**, 181 (2001).

[29] D. Bachner *et al.*, Nucl. Phys. **A99**, 487 (1967).

[30] R. M. Britton and D. L. Watson, Nucl. Phys. **A272**, 91 (1976).

[31] P. Roussel, G. Bruge, A. Bussiere, H. Faraggi, and J. E. Testoni, Nucl. Phys. **A155**, 306 (1970).

[32] A. L. McCarthy and G. M. Crawley, Phys. Rev. **150**, 935 (1966).

[33] W. M. Stewart and K. K. Seth, NASA-TN-D-7354 (1973).

[34] J. H. Bjerregaard, O. Nathan, S. Hinds, and R. Middleton, Nucl. Phys. **85**, 593 (1966).

[35] S. A. Hjorth and L. H. Allen, Ark. Fys. **33**, 207 (1967).

[36] A. G. Hartas, C. T. Papadopoulos, P. A. Assimakopoulos, N. H. Gangas, and G. Andritsopoulos, Nucl. Phys. **A279**, 413 (1977).

[37] B. Erlandsson, K. Nilson, A. Marcinkowski, and J. Piotrowski, Z. Phys. A **293**, 43 (1979).

[38] B. Zeidman and J. A. Nolen, Jr, Phys. Rev. C **18**, 2122 (1978).

[39] A. M. Oros-Peusquens and P. F. Mantica, Nucl. Phys. **A669**, 81 (2000).

[40] I. Stefanescu *et al.*, Phys. Rev. Lett. **100**, 112502 (2008).

[41] Takaharu Otsuka, Toshio Suzuki, Rintaro Fujimoto, Hubert Grawe, and Yoshinori Akaishi, Phys. Rev. Lett. **95**, 232502 (2005).

[42] S. Juutinen, J. Hattula, M. Jääskeläinen, A. Virtanen, and T. Lönnroth, Nucl. Phys. **A504**, 205 (1989).

[43] C. Andreoiu *et al.*, Eur. Phys. J. A **14**, 317 (2002).

[44] T. Ishii, M. Asai, A. Makishima, I. Hossain, M. Ogawa, J. Hasegawa, M. Matsuda, and S. Ichikawa, Phys. Rev. Lett. **84**, 39 (2000).

[45] L.-L. Andersson *et al.*, Eur. Phys. J. A **36**, 251 (2008).

[46] O. M. Mustaffa, L. P. Ekström, G. D. Jones, F. Kearns, T. P. Morrison, H. G. Price, D. N. Simister, P. J. Twin, R. Wadsworth, and N. J. Ward, J. Phys. G: Nucl. Phys. **5**, 1283 (1979).

[47] Bai Erjun and Huo Junde, Nucl. Data Sheets **92**, 147 (2001).

[48] Ole Hansen, M. N. Harakeh, J. V. Maher, L. W. Put, and J. C. Vermeulen, Nucl. Phys. **A313**, 95 (1979).

[49] A. Jokinen *et al.*, EPJdirect **A3**, 1 (2002).

[50] Coral M. Baglin, Nucl. Data Sheets **95**, 215 (2002).

[51] M. R. Bhat, Nucl. Data Sheets **88**, 417 (1999).

[52] M. R. Bhat and J. K. Tuli, Nucl. Data Sheets **90**, 269 (2000).

[53] Khalifeh Abusaleem and Balraj Singh, Nucl. Data Sheets **112**, 133 (2011).

[54] Huo Junde, Huo Su, and Yang Dong, Nucl. Data Sheets **112**, 1513 (2011).

[55] Caroline D. Nesaraja, Scott D. Geraedts, and Balraj Singh, Nucl. Data Sheets **111**, 897 (2010).

[56] J. K. Tuli, Nucl. Data Sheets **100**, 347 (2003).

[57] Huo Junde and Balraj Singh, Nucl. Data Sheets **91**, 317 (2000).

[58] Balraj Singh, Nucl. Data Sheets **108**, 197 (2007).

[59] E. Browne and J. K. Tuli, Nucl. Data Sheets **111**, 1093 (2010).

[60] T. W. Burrows, Nucl. Data Sheets **97**, 1 (2002).

[61] J. K. Tuli, Nucl. Data Sheets **103**, 389 (2004).

[62] Evaluated Nuclear Structure Data File (ENSDF) [http://www.nndc.bnl.gov/ensdf].

[63] J. Leske, K.-H. Speidel, S. Schielke, O. Kenn, D. Hohn, J. Gerber, and P. Maier-Komor, Phys. Rev. C **71**, 034303 (2005).

[64] J. Leske, K.-H. Speidel, S. Schielke, J. Gerber, P. Maier-Komor, T. Engeland, and M. Hjorth-Jensen, Phys. Rev. C **72**, 044301 (2005).

[65] P. Boutachkov *et al.*, Phys. Rev. C **75**, 021302(R) (2007).

[66] R. E. Shroy, A. K. Gaigalas, G. Schatz, and D. B. Fossan, Phys. Rev. C **19**, 1324 (1979).

[67] E. Caurier, shell-model code ANTOINE, IRES, Strasbourg 1989-2004; Etienne Caurier and Frederic Nowacki, Acta Phys. Pol. B **30**, 705 (1999).

[68] B. A. Brown, private communication; see also the endnote [28] in B. Cheal *et al.*, Phys. Rev. Lett. **104**, 252502 (2010).

[69] S. Zhu *et al.*, Phys. Rev. C (submitted).

[70] Tsan Ung Chan, J. F. Bruandet, B. Chambon, A. Dauchy, D. Drain, A. Giorni, F. Glasser, and C. Morand, Nucl. Phys. **A348**, 179 (1980).

[71] S. Franchoo *et al.*, Phys. Rev. C **64**, 054308 (2001).

[72] T. Pawłat *et al.*, Nucl. Phys. **A574**, 623 (1994).

TABLE III: Properties of levels and gamma rays in ^{65}Cu. The gamma-ray intensities I_γ are normalized to 100 for the strongest transition. The AD coefficients a_2 and a_4 were deduced from the ^{48}Ca + ^{26}Mg data [26]. Entries of "$a_4 \equiv 0$" imply that this coefficient was constrained to avoid an unphysical or unreliable result. Transition multipolarities are assigned based on the AD results, from known literature values [17], or inferred from the level scheme. For $M1/E2$ transitions, approximate mixing ratios δ were also obtained.

E_{level} (keV)	I^π	E_γ (keV)	I_γ	a_2	a_4	Multipolarity
0.0	$3/2^-$					
1115.6	$5/2^-$	1115.5(1)	91(9)	−0.37(5)	0.03(5)	$\Delta I = 1$ $M1/E2$ $(\delta = -0.1)$
1481.8	$7/2^-$	366.3(5)	16.6(5)	−0.23(7)	0.00(9)	$\Delta I = 1$ $M1/E2$ $(\delta = 0.0)$
		1481.8(1)	91(12)			$E2$
1623.6	$5/2^-$	507.9(10)	7(4)			$\Delta I = 0$ $M1/E2$
		1623.8(3)	12(9)			$\Delta I = 1$ $M1/E2$
2094.1	$7/2^-$	470.5(5)	7(4)			$\Delta I = 1$ $M1/E2$
		612.1(2)	18.2(5)	−0.45(32)	$\equiv 0$	$\Delta I = 0$ $M1/E2$
		978.5(1)	53.7(16)	0.21(3)	−0.06(4)	$\Delta I = 1$ $M1/E2$ $(\delta = +0.4)$
		2094.2(1)	31.8(7)			$E2$
2279.1	$7/2^-$	(656)	(∼5)			$(\Delta I = 1$ $M1/E2)$
		1163.5(1)	31(4)			$\Delta I = 1$ $M1/E2$
2406.1	$(7/2, 9/2)^-$	312.1(5)	11.8(4)			$(M1/E2)$
		924.3(1)	27.3(5)			$(M1/E2)$
		1290.6(1)	18(9)			
2533.6	$9/2^+$	254.5(1)	25.5(6)	−0.25(5)	0.00(7)	$\Delta I = 1$ $E1$
		439.5(1)	100(3)	−0.17(3)	0.04(4)	$\Delta I = 1$ $E1$
		1052.1(1)	91(2)	−0.21(20)	−0.03(23)	$\Delta I = 1$ $E1$
		2534.1(10)	7.0(13)			$E3$
2998.1	$11/2^-$	591.9(1)	32(9)			
		1516.2(2)	8.2(3)			$E2$
3547.6	$(11/2)^+$	1014.1(2)	19(3)			$(\Delta I = 1$ $M1/E2)$
3659.6	$13/2^+$	661.5(1)	31.8(12)	−0.14(11)	0.04(12)	$\Delta I = 1$ $E1$
		1126.1(1)	77(3)	0.18(5)	−0.03(6)	$E2$

TABLE III: *(Continued.)*

E_{level} (keV)	I^π	E_γ (keV)	I_γ	a_2	a_4	Mult.
4006.3	$13/2^+$	458.4(7)	5(2)			$(\Delta I = 1\ M1/E2)$
		1472.8(1)	16(3)			$E2$
4074.5	$(15/2)^+$	414.8(1)	68.2(11)	0.15(3)	0.00(4)	$(\Delta I = 1\ M1/E2)$
		527.4(3)	4.5(2)	0.03(10)	$\equiv 0$	$(E2)$
4355.7	$17/2^+$	281.1(1)	30.9(5)	0.20(2)	$-0.05(2)$	$(\Delta I = 1\ M1/E2)$ $(\delta = +0.4)$
		350.0(3)	7(3)	0.33(13)	$\equiv 0$	$E2$
		696.6(5)	32.7(4)	0.25(18)	$\equiv 0$	$E2$
4936.3		861.8(1)	16.4(14)	$-0.63(11)$	$\equiv 0$	$M1/E2$
5485.8		549.5(2)	6(2)	$-0.29(16)$	$\equiv 0$	
		1130.1(1)	8.2(5)			
6233.0		747.2(2)	5(2)			

TABLE IV: Properties of levels and gamma rays in ^{67}Cu. The gamma-ray intensities I_γ are normalized to 100 for the strongest transition. The AC coefficients a_2 and a_4 were deduced from the ^{64}Ni + ^{238}U data. Entries of "$a_4 \equiv 0$" imply that this coefficient was constrained to avoid an unphysical or unreliable result. Transition multipolarities are assigned based on the AC results, from known literature values [18], or inferred from the level scheme. For $M1/E2$ transitions, approximate mixing ratios δ were also obtained. In cases where an AC could be fitted using two different gates, both results are given in the table.

E_{level} (keV)	I^π	E_γ (keV)	I_γ	a_2	a_4	Multipolarity
0.0	$3/2^-$					
1115.1	$5/2^-$	1114.9(1)	42(4)	−0.13(3)	$\equiv 0$	$\Delta I = 1$ $M1/E2$ $(\delta = -0.19)^a$
1669.4	$7/2^-$	554.1(1)	46(4)	−0.12(7)	$\equiv 0$	$\Delta I = 1$ $M1/E2$ $(\delta = -0.11)^a$
				0.24(3)	0.03(5)	$\Delta I = 1$ $M1/E2$ $(\delta = -0.15)^b$
		1669.5(1)	39(4)	0.10(4)	0.06(6)	$E2^a$
2361.3	$7/2^-$	691.7(2)	4.2(4)			$\Delta I = 0$ $M1/E2$
		1246.0(1)	41(2)	0.16(5)	$\equiv 0$	$\Delta I = 1$ $M1/E2$ $(\delta = -0.07)^c$
		2360.9(4)	4.7(6)			$E2$
2502.6	$9/2^+$	833.1(1)	97(3)			$E1$
		1387.2(1)	10.4(3)			$M2$
		2502.8(1)	59(2)			$E3$
2932.9	$9/2^-$	571.5(1)	30(2)	−0.09(3)	$\equiv 0$	$\Delta I = 1$ $M1/E2$ $(\delta = +0.25)^d$
		1818.2(1)	4.2(2)			$E2$
2984.2		1314.3(2)	3.3(12)			
		1869.7(3)	4(4)			
3116.1		613.5(5)	10(4)			
(3296.0)	$(11/2)^+$	793.3(1)	12(4)	0.29(12)	0.08(17)	$(\Delta I = 1$ $M1/E2)$ $(\delta = +1.9)^e$
3363.3	$13/2^+$	(67)	∼10			$(\Delta I = 1$ $M1/E2)$
		860.5(1)	100(3)	0.18(4)	0.09(6)	$E2^e$
3431.3	$11/2^-$	498.3(1)	19(2)	0.06(6)	$\equiv 0$	$\Delta I = 1$ $M1/E2$ $(\delta = +0.03)^b$
				0.11(7)	$\equiv 0$	$\Delta I = 1$ $M1/E2$ $(\delta = -0.06)^d$
		1070.3(1)	7.0(10)			$E2$
		1762.2(1)	6.3(2)			$E2$

TABLE IV: *(Continued.)*

E_{level} (keV)	I^π	E_γ (keV)	I_γ	a_2	a_4	Mult.
3463.2	$15/2^+$	99.9(1)	77(4)	−0.04(12)	0.12(18)	$\Delta I = 1\ M1/E2^e$
3518.8	$(9/2^-)$	534.3(10)	2(1)			
		1849.4(2)	6(4)	−0.16(12)	0.05(18)	$(\Delta I = 1\ M1/E2)^f$
3631.8		647.6(3)	2.1(8)			
		699.4(5)	2.9(12)			
3987.7	$(17/2)^+$	524.4(1)	37(4)	0.20(2)	−0.06(3)	$(\Delta I = 1\ M1/E2)\ (\delta = +1.6)^a$
				0.47(4)	0.09(6)	$(\Delta I = 1\ M1/E2)\ (\delta = +1.0)^e$
		624.5(1)	17(2)	0.19(9)	$\equiv 0$	$(E2)^e$
4016.0	$(13/2^-)$	584.6(1)	10(2)			$(\Delta I = 1\ M1/E2)$
		1083.1(2)	3.2(8)			$(E2)$
4176.9		713.7(2)	3(2)	0.11(21)	$\equiv 0$	^{e}
4299.5	$(13/2^-)$	283.5(5)	2.5(7)			$(\Delta I = 0\ M1/E2)$
		667.8(2)	2.1(8)			
		780.8(1)	6(2)	0.11(16)	$\equiv 0$	$(E2)^f$
		868.2(1)	15.2(14)			$(\Delta I = 1\ M1/E2)$
4690.4	$(15/2^-)$	674.1(2)	4(2)			$(\Delta I = 1\ M1/E2)$
		1259.1(1)	6.6(7)			$(E2)$
4762.7	$(15/2)$	463.3(1)	20(4)			
		774.8(1)	34.2(10)	−0.02(3)	0.01(5)	$dipole^a$
				−0.07(6)	$\equiv 0$	$dipole^e$
4934.7		244.3(1)	5.0(8)			
		(919)	(∼4)			
4979.8		802.9(2)	3.1(4)	0.20(22)	$\equiv 0$	^{e}
5336.3		401.6(1)	4.6(11)			
5748.4		985.8(2)	6(4)			

TABLE IV: *(Continued.)*

E_{level} (keV)	I^π	E_γ (keV)	I_γ	a_2	a_4	Mult.
5848.6		512.3(3)	2(1)			
5887.6		1124.9(1)	11(2)			
6285.6		1522.9(1)	7.6(6)			

[a]From AC with 861-keV $E2$ gating transition.

[b]From AC with 1115-keV $M1/E2$ ($\delta = -0.19$) gating transition.

[c]From $1246 - 1115$ AC, with gate placed on the former transition.

[d]From AC with 1246-keV $M1/E2$ ($\delta = -0.07$) gating transition.

[e]From AC with 2503-keV $E3$ gating transition.

[f]From AC with 1670-keV $E2$ gating transition.